

1 ***Circadian clock mechanism driving mammalian photoperiodism***

2

3 Wood S.H.^{1,2,8}, Hindle, M.M.^{3,8}, Mizoro, Y.¹, Cheng, Y.^{4,5}, Saer B.R.C.¹,
4 Miedzinska K.³, Christian H.C.⁶, Begley, N.¹, McNeilly J.⁷, McNeilly A.S.⁷,
5 Meddle, S.L.³, Burt, D.W.^{3,4}, Loudon A.S.I.^{1*}

6

7 ¹ Centre for Biological Timing, Faculty of Life Sciences, University of
8 Manchester, Manchester M13 9PT, UK

9 ² Arctic Chronobiology and Physiology research group, Department of Arctic
10 and Marine Biology, UiT – The Arctic University of Norway, Tromsø NO-9037,
11 Norway

12 ³ The Roslin Institute, and Royal (Dick) School of Veterinary Studies
13 University of Edinburgh, Roslin, Midlothian EH25 9PRG, UK

14 ⁴ UQ Genomics Initiative, The University of Queensland, Brisbane, QLD 4072,
15 Australia

16 ⁵ School of Life and Environmental Sciences, Faculty of Science, The
17 University of Sydney, New South Wales, Australia

18 ⁶ University of Oxford, Department of Physiology, Anatomy and Genetics, Le
19 Gros Clark Building, South Parks Road, Oxford, OX1 3QX, UK

20 ⁷ MRC Centre for Reproductive Health, Queen's Medical Research Institute,
21 Edinburgh EH16 4TJ, UK

22 ⁸ These authors contributed equally

23 *Corresponding author: andrew.loudon@manchester.ac.uk

24 **Abstract**

25 The annual photoperiod cycle provides the critical environmental cue
26 synchronizing rhythms of life in seasonal habitats. In 1936, Bünning proposed
27 a circadian-based coincidence timer for photoperiodic synchronization in
28 plants. Formal studies support the universality of this so-called coincidence
29 timer, but we lack understanding of the mechanisms involved. Here we show
30 in mammals that long photoperiods induce the circadian transcription factor
31 *BMAL2*, in the *pars tuberalis* of the pituitary, and triggers summer biology
32 through the eyes absent / thyrotrophin (EYA3 / TSH) pathway. Conversely,
33 long-duration melatonin signals on short photoperiods induce circadian
34 repressors including *DEC1*, suppressing *BMAL2* and the EYA3/TSH pathway,
35 triggering winter biology. These actions are associated with progressive
36 genome-wide changes in chromatin state, elaborating the effect of the
37 circadian coincidence timer. Hence, circadian clock-pituitary epigenetic
38 pathway interactions form the basis of the mammalian coincidence timer
39 mechanism. Our results constitute a blueprint for circadian-based seasonal
40 timekeeping in vertebrates.

41 INTRODUCTION

42 The annual photoperiod cycle provides a critical predictive environmental cue
43 driving annual cycles of fertility, physiology and behaviour in most animal
44 species. In 1936, Erwin Bünning proposed the external coincidence
45 hypothesis for a circadian-based timing mechanism driving photoperiodic
46 responses in plants ¹. The proposition was that photoperiod entrains a
47 circadian rhythm of photosensitivity, and the expression of summer or winter
48 biology depends on whether or not light coincides with the phase of high
49 photosensitivity. An internal coincidence model has also been proposed
50 where the role of light is to entrain two circadian oscillators and the phase
51 relationship between the two oscillators determines the response to
52 photoperiod ^{2,3}. In either case the role of the circadian clock is central and
53 formal studies support the universality of a coincidence timer in animals ²⁻⁷,
54 but we lack understanding of the mechanisms involved.

55 In mammals, the duration of the night-time pineal melatonin signal is sculpted
56 by the photoperiod and is a critical regulator of annual cycles of reproduction,
57 growth and metabolism ⁸⁻¹⁴. The melatonin signal is decoded within the *pars*
58 *tuberalis* (PT) of the pituitary gland ^{9,13,15-18}. Day-length dependent changes
59 in hypothalamic thyroid hormone (TH) metabolism control the seasonal
60 changes in physiology and are regulated via the PT, through altered secretion
61 of thyrotrophin (TSH) ¹⁹⁻²¹. This TSH circuit is specific to the PT, and distinct
62 from that in the anterior pituitary, which controls normal thyroid gland function.
63 LP-activation of PT-TSH depends on regulation of TSH β subunit expression
64 by the transcriptional co-activator, EYA3, which operates as a TSH on-switch.
65 EYA3 co-activates the PAR bZIP Transcription Factor TEF (thyrotroph
66 embryonic factor) via a D-box element on the *TSH β* promoter ²²⁻²⁴ (Fig. 1a).
67 This prior work places EYA3 at the centre of photoperiodic time measurement
68 within the melatonin target tissue, but does not explain how expression is
69 regulated by the seasonal clockwork.

70 In addition to acute circadian-based mechanisms an epigenetic basis to
71 longer-term seasonal control in flowering in plants is well established.
72 Specifically, the duration of cold temperatures during the winter season alters

73 chromatin accessibility at key genes, and is a requirement for full photoperiod
74 induced flowering (vernalisation)²⁵⁻²⁷. In animals, no evidence for dynamic
75 genome-wide seasonal epigenetic regulation of transcription has been
76 described.

77 Here, we show that coincidence timing depends on a flip-flop switch between
78 the expression of the circadian genes *BMAL2*, (a parologue of the circadian
79 regulator *BMAL1*) and *DEC1*, and their respective activating or suppressive
80 effects on *EYA3* in the PT. The duration of the melatonin signal is key in
81 sculpting these molecular components. Additionally, the effect of the
82 coincidence timer is elaborated by progressive genome-wide changes in
83 epigenetic status at key seasonal gene promoters. Therefore, circadian clock
84 interactions with pituitary epigenetic pathways form the basis of the
85 mammalian coincidence timer mechanism.

86 **RESULTS**

87 ***Epigenetic regulation of the seasonal transcriptome***

88 Seasonally breeding sheep are a well-established photoperiodic model for the
89 study of neuroendocrine mechanisms underpinning seasonal physiology
90^{14,28,29}. Using a study design that compared the effects of transfer from long
91 photoperiod (LP) to short photoperiod (SP) with transfer from SP to LP (Fig.
92 1b), we collected *pars tuberalis* (PT) tissue at 1,7 and 28 days after transfer,
93 with collections timed for 4-h after lights on (ZT4), when *EYA3* expression
94 peaks under LP^{22,24,29}. Changes in prolactin concentrations²⁹⁻³¹ confirmed
95 photoperiodic hormone responses (Fig. 1b, n=28), as well as LP activation of
96 *EYA3*, and inverse expression patterns of *TSHβ* (LP marker) and *CHGA* (SP
97 marker) (Supplementary Fig. 1a-d, n=4), validating this paradigm.

98 Comparing LP day 28 to SP day 28 by electron microscopy we found an
99 increased nuclear diameter, equating to an approximate doubling in volume of
100 PT thyrotrophs, and a marked reduction in chromatin density on LP (Fig. 1c,
101 Supplementary Fig. 1e & f). These morphological changes were not seen in
102 *Pars distalis* (PD) somatotrophs but were observed in the PT follicular stellate
103 (FS) cells to a lesser degree (Fig. 1c, Supplementary Fig. 1e & f). We
104 hypothesized that increased chromatin accessibility may account for the
105 photoinductive effects of LP and therefore changes in the seasonal
106 transcriptome.

107 Comparing all seasonal time-points (Fig. 1b, red arrows) we performed ChIP-
108 seq (histone marker H3K4me3, Supplementary Data 1 & 2, n=2) and RNA-
109 seq (Supplementary Data 3, n=3) to screen for seasonal transcriptional
110 activation. To determine if epigenetic changes in H3K4me3 marks were
111 associated with transcriptional activation we first improved the sheep genome
112 annotation of transcripts and transcription start sites (TSS) with PT RNA and a
113 combination of Cap Analysis of Gene Expression (CAGE-seq, Supplementary
114 Data 4)³² and ISOSEQ long-read RNA-seq (SRA: PRJNA391103, see
115 methods for details). Using this improved annotation we identified H3K4me3
116 peaks and found the distribution on genomic features to be similar to previous
117 studies³³⁻³⁵, validating our approach (see methods section).

118 Next we identified seasonally expressed genes, as defined by RNA-seq
119 analysis of differentially regulated genes (DEGs) in the SP to LP and LP to SP
120 transfers (Supplementary Data 3), and observed a strong correlation between
121 seasonal gene expression and H3K4me3 peaks around the transcription start
122 sites (TSS's)(Fig. 1d). Importantly, this correlation was absent in non-
123 seasonally regulated genes and we found the distributions between seasonal
124 and non-seasonally regulated genes to be significantly different (Fig. 1d, P
125 value < 0.001 Mann-Whitney U test). Histone modifications are precisely
126 balanced by methyltransferases (writers), demethylases (erasers) and effector
127 proteins (readers), therefore we checked the RNA expression of H3K4me3
128 readers, writers and erasers but found no seasonal changes (Supplementary
129 Data 5). This suggests that changes in protein activity of H3K4me3
130 modulators may be key in the observed seasonal alterations of H3K4me3
131 marks.

132 We noted that approximately 70% of seasonally DEGs (Supplementary Data
133 3) had more than one TSS compared to only ~20% of the PT genomic
134 background (Supplementary Fig. 1g, Supplementary Data 4). Next we took
135 genes that were up-regulated in either SP or LP and plotted the proportion of
136 genes with multiple TSS's, and repeated this for H3K4me3 marked TSS's, this
137 revealed that H3K4me3 marks are more likely to occur on genes with multiple
138 TSS's and highly expressed seasonal DEGs have a greater prevalence of
139 multiple TSSs than non-seasonal genes expressed at the same level (Fig. 1e).
140 Furthermore, this phenomenon was more pronounced in LP than SP. This
141 indicates that LP up-regulated genes are more likely to have multiple TSS's
142 and be associated with the H3K4me3 mark.

143 To investigate which promoter motifs may be actively transcribed we searched
144 for enriched transcription factor binding site motifs in the TSS's marked with
145 H3K4me3 in the LP day 28 vs SP day 28 comparison (Fig. 1f, Supplementary
146 Fig. 2a & b). This showed enrichment of D-box binding motifs, Basic Leucine
147 Zipper ATF-Like transcription related factors and POU domains for in both the
148 up and down-regulated genes (Fig. 1f).

149 *TSHβ*, an exemplar seasonal D-box regulated gene^{22,23}, revealed progressive
150 activation by LP, correlated with expression, and with no detectable H3K4me3
151 mark at either SP day 28 or 84 (R=0.961, p-value=0.002, Fig. 2a, b). In
152 contrast, CHGA revealed an inverse seasonal pattern (R=0.843, p-
153 value=0.009, Supplementary Fig. 2c, d). Global enrichment of D-box sites on
154 LP-activated genes indicates a potentially extensive role for TEF, SIX1 and
155 EYA3 co-activation in seasonal regulation of physiology, and strongly focuses
156 attention on the regulation of EYA3.

157 In line with our global analysis showing the presence of multiple TSSs in
158 seasonally expressed genes we identified two transcription start sites in *EYA3*,
159 an up-stream TSS with non-canonical E-boxes and a downstream TSS
160 containing two paired canonical E-Boxes²² (Fig. 2c). CAGE analysis revealed
161 that only the down-stream TSS was actively transcribed on LP (Fig. 2c,
162 Supplementary Data 4). We correlated RNA expression with H3K4me3 marks
163 for both TSS's, which confirmed seasonal regulation specific to the down-
164 stream TSS (*EYA3* downstream TSS: R=0.778, P=0.02, Fig. 2d, *EYA3*
165 upstream TSS: R=0.308, P=0.46, Supplementary Fig. 2e & f). Next, we cloned
166 each *EYA3* TSS into luciferase reporters, and using COS7 cells transfected
167 the reporters along with known E-box regulators^{22,23} (see methods for details).
168 This revealed significant activation specific to the downstream (seasonal) TSS
169 (Supplementary Fig. 2g), likely due to the presence of multiple canonical e-
170 box pairs.

171

172 ***BMAL2* an activator in a circadian-based coincidence timer**

173 The E-box regulators *CLOCK* and *BMAL1* do not show significant changes in
174 amplitude in the PT under different photoperiods^{22,36}, therefore we aimed to
175 identify a candidate circadian E-box regulator of the *EYA3* downstream TSS.
176 The prediction is that a circadian E-box regulator, would peak in expression
177 only when light falls on the photosensitive phase, as in the early light phase of
178 LP (approx. ZT4), and would be absent on SP where the photosensitive
179 phase is masked by darkness. The RNA-seq dataset revealed progressive up-

180 regulation by LP of multiple transcripts, and a slower inverse pattern on SP
181 (Fig. 3a, Supplementary Data 3).

182

183 Importantly these data identified *BMAL2*, an E-box regulator and parologue of
184 *BMAL1*, as progressively up-regulated on LP (Fig. 3a & b), closely matching
185 the expression profile for *EYA3* (Fig. 3b). We tested whether *BMAL2* was
186 capable of activating the downstream *EYA3* TSS (Supplementary Fig. 2h). In
187 the presence of *CLOCK*, or alone, *BMAL2* had a weak non-significant effect,
188 but in the presence of *BMAL1* and *CLOCK*, we observed significant 4 to 5-fold
189 activation (Supplementary Fig. 2h, Fig. 3c). We then tested whether this
190 depended on direct E-box binding by *BMAL2*, by mutating the *BMAL2* DNA-
191 binding domain (arginine of basic helix-loop-helix domain to alanine R88A³⁷),
192 and observed near-identical augmentation of *EYA3* expression (Fig. 3d). The
193 observation that transcription factors can act as co-activators³⁸ and that
194 bHLH circadian transcription factors require internal PAS domains for
195 functional protein-protein interactions³⁹, with PAS-B an essential domain for
196 *BMAL1* protein-protein interactions⁴⁰ led us to mutate the PAS-B domain on
197 ovine *BMAL2* (F427R_V439R)⁴⁰. This significantly impaired *EYA3* activation,
198 blocking the co-activation effect with *BMAL1* and *CLOCK* (Fig. 3e). This
199 suggests that *BMAL2* operates as a co-activator of *EYA3*, in a
200 *CLOCK/BMAL1*-dependent manner, requiring PAS-B dependent protein-
201 protein interactions for the mechanism of action, confirmation of this will
202 require suitable antibodies to be raised for future studies.

203 We assessed the daily profile of *BMAL2* by in-situ hybridization, using
204 archived material²⁴. This revealed strong LP-dependent induction of *BMAL2*
205 in the early light phase (ZT3, Fig. 3f), and flat low 24h expression on SP.
206 Collectively this reveals that *BMAL2* operates as a co-activator driving
207 photoperiodic responses, and fulfils the criteria as a candidate activating arm
208 of the circadian-based coincidence timer.

209

210 ***Circadian clock repressors shut-down the LP transcriptome***

211 A prediction from a coincidence timer model is that repressive mechanisms
212 would emerge on short photoperiods in the late night (i.e. photo-inducible

213 phase masked by darkness). To assess this we conducted a serial RNA-seq
214 experiment on PT tissue collected over at 4-hour intervals from both SP and
215 LP-housed animals (Day 28 Fig. 1b & Fig. 4a). Transcripts at the two ZT0
216 collections 24h apart (ZT0 and ZT24) in each photoperiod had virtually
217 identical RNA-seq profiles, validating dissection technique and down-stream
218 analyses (Supplementary Fig. 3a & Supplementary Data 6). We identified
219 transcripts that significantly changed across the day (diurnal genes) within
220 each photoperiod, and defined the phase, amplitude and period ⁴¹
221 (Supplementary Data 6). More transcripts were rhythmic on SP compared to
222 LP (SP = 880, LP = 643 (Fig. 4b)), with striking asymmetry in the peak phase
223 of expression on both SP and LP (Fig. 4c). Large numbers of genes were
224 expressed on SP in late night (ZT20, 24) and on LP in the early light phase
225 (ZT4; Fig. 4c), and surprisingly relatively few genes common to both
226 photoperiods (250 transcripts, Fig. 4b & d), but shared genes included the
227 canonical clock genes (Supplementary Fig. 3b).

228 Amongst diurnal genes shared across photoperiods, dawn-peaking clusters
229 were enriched for the GO term cAMP binding activity, while the dark-onset
230 cluster was marked by the circadian suppressor *CRY1* ^{42–44} (Fig. 4d & e,
231 Supplementary Fig. 3c). Previous studies have shown *CRY1* is directly
232 induced by onset of melatonin secretion ^{17,45–47} and that the pattern of
233 induction does not alter between photoperiods. We also observed that
234 regulators of *CRY1* protein stability, *FBXL3* and *FBXL21* ^{22,48,49}, are
235 expressed in the PT, but here there were marked photoperiod-dependent
236 changes in phasing for *FBXL21* (Fig. 4e) .

237 *BMAL2* emerged as the only transcription factor, which showed both phase
238 and amplitude changes in expression on LP (Fig. 4e, Supplementary Data 6).
239 On LP there was a 4 log-fold increase in expression of *BMAL2*, with bi-phasic
240 peaks at ZT4 and ZT20. In contrast, *BMAL1* showed no alteration in amplitude
241 of expression, on either SP or LP (Fig. 4e).

242 At SP ZT20 we noted a strong functional enrichment for the terms negative
243 regulation of transcription, E-box binding and co-repressor activity
244 (Supplementary Fig. 3c & d). Within this group, we identified 8 genes with

245 known circadian repressor function (*REVERB- α* , *DEC1*, *DEC2*, *CHRONO*,
246 *FBXL21*, *KLF10*, *JUNB*, *GATA2* and *ERF*, Fig. 4e & Supplementary Fig. 3e).
247 Notably 6 are circadian clock components acting through E-boxes. Cistromic
248 analysis identified over-representation of circadian RORE, D-Box and E-Box
249 sites on the proximal promoter regions in late-night genes on SP (ZT20) and
250 on LP at the dark-light transition (Fig. 4f). Cluster analysis revealed 4 major
251 clusters of E-box motif-enriched genes associated with late night and dawn
252 transition on SP (ZT20) and LP (ZT4) respectively, with *BMAL2* contained
253 within the LP ZT4 cluster (Fig. 4g), and circadian repressor elements within
254 the SP ZT20 peaking cluster (Fig. 4g). This led us to ask; are SP ZT20
255 repressors more likely to interact, and therefore potentially repress, LP ZT4
256 up-regulated genes. We used curated experimental protein-protein interaction
257 (PPI) observations from the STRING database, which contain known protein-
258 protein interactions and functional associations⁵⁰. We found that LP ZT4 up-
259 regulated genes are more enriched within the SP ZT20 repressor network (P-
260 value = 0.001) than down-regulated genes (Supplementary Fig 4a, b). We did
261 not find significant enrichment when considering genes that are differentially
262 up or down regulated across the whole day (P-value = 0.25) (Supplementary
263 Fig. 4b). This suggests that SP is defined by an up-regulation of
264 transcriptional repressors responsible for the suppression of the LP activated
265 transcriptome.

266 ***Melatonin-regulated circadian repression***

267 Earlier studies have defined the role for melatonin both as an acute inducer of
268 *CRY1*^{17,36,45,47}, but also determined clear melatonin duration-dependent
269 effects for photoperiodic responses^{8,51}. Our data suggest that prolonged SP-
270 like signals may trigger late-night induction of a separate cohort of circadian
271 repressors genes. To test this, we maintained a cohort of animals on LP and
272 then transferred animals to constant light (LL), a regimen known to suppress
273 the endogenous rise in pineal melatonin secretion⁵². Simultaneously, and at
274 the time of normal lights off (i.e. expected onset of the melatonin signal) we
275 treated animal with an intradermal Regulin melatonin implant⁴⁷, which mimics
276 the endogenous dark-onset rise of this hormone⁵³, validated by RIA for
277 melatonin (Supplementary Fig. 5a, n=6). PT tissue was collected for in-situ

278 hybridization analysis at +1.5 hours (ZT17.5), +3.5 hours (ZT19.5), +6.5 hours
279 (ZT22.5) and +9.5h after hormone treatment, the latter time point being
280 equivalent to 1.5 hours into the predicted light-onset phase on LP (i.e. ZT1.5;
281 Fig. 5a, n=4).

282 *CRY1* expression in the PT was completely suppressed by constant light, but
283 rapidly induced by melatonin treatment, as previously observed ^{17,45-47} (Fig.
284 5b). By ZT1.5, expression levels had dropped to basal. In LL conditions *DEC1*,
285 *REVERB α* and *CHRONO* were rapidly elevated in the early subjective dark
286 phase, and in an abnormal pattern when compared to endogenous profiles in
287 LP conditions (Fig. 4e vs Fig 5c-e). In marked contrast, exposure to melatonin
288 initially repressed all 3 genes, which peaked at +9.5h, equivalent to ZT1.5 on
289 LP (Fig.s 5c - e). For *DEC1* and *CHRONO*, this pattern closely resembled the
290 phase of the endogenous rise of these genes in animals housed in SP
291 photoperiods (Fig. 4e & 5f). From this, we conclude that multiple repressor
292 arms of the circadian clock are direct melatonin targets and act as a read-out
293 of long duration melatonin signals. This defines a molecular basis for a
294 hormone-regulated circadian-based coincidence timer mechanism, capable of
295 discriminating LP and SP responses within the melatonin target tissue.

296 ***DEC1 suppression of BMAL2-mediated EYA3 activation***

297 *DEC* proteins are known E-box suppressors of the circadian clock ^{54,55}, so we
298 selected *DEC1* for further analysis. Quantitative in-situ hybridization confirmed
299 the temporal pattern of *DEC1* expression (Fig. 5f) in the PT, and using
300 immunohistochemistry of short-photoperiod derived PT tissue, we showed co-
301 localisation of *DEC1* protein to α GSU expressing thyrotroph cells in the PT
302 (Fig. 5g). *DEC1* appears to be specific to thyrotrophs, and was not detected in
303 a common cell-type in the PT, the folliculo-stellate cells. We cloned ovine
304 *DEC1*, and then tested action on BMAL2-mediated induction of *EYA3*. This
305 showed that *DEC1* significantly suppressed the action of both CLOCK
306 /BMAL1 (Supplementary Fig. 5b & c) and CLOCK/BMAL1/BMAL2-mediated
307 expression of *EYA3* (Fig. 5h, Supplementary Fig. 5c). We also tested *DEC2*,
308 which was without effect (Supplementary Fig. 5d). Hence, *DEC1* and BMAL2
309 exert mutually antagonistic effects on *EYA3* expression.

310 Discussion

311 Our study reveals a circadian coincidence timer within the PT, sculpted by the
312 nocturnal melatonin signal that encodes the mammalian photoperiodic
313 response (Fig. 6). Under LP, *BMAL2* exhibits a high-amplitude peak timed
314 approximately 12h after the onset of the preceding dark phase, coincident with
315 expression of *EYA3* in the early light phase ²². This 12h interval from dark
316 onset to the dawn peak is also remarkably close to the critical photoperiod
317 required to activate a long-day response in sheep ^{28,56}. We note that both
318 *BMAL2* and *EYA3* show a second peak on day 28 of LP, however, these
319 peaks are “dysynchronised” (ZT20 *BMAL2* and ZT15/16 *EYA3* ²⁴).
320 Furthermore, the second peak in *EYA3* expression is absent in early
321 responses to LP ²² indicating that it is potentially not mechanistically
322 important in a coincidence model. We show that *BMAL2* acts as a co-activator
323 of *EYA3* with *CLOCK* and *BMAL1*, likely in a complex through the PAS-B
324 domain interaction ⁵⁷. Co-activators are recognized as important rapid-
325 response functional integrators of multiple transcription factors, driving distinct
326 biological programmes and environmental responses, including adaption to
327 cold, rapid diet change and disease ³⁸. Within the PT, *BMAL2* and *EYA3* may
328 therefore operate as a photoperiodic co-activator cascade. It remains unclear
329 how *BMAL2* is regulated, and current models for the regulation of *BMAL2* by
330 *BMAL1* may not be applicable ⁵⁸. Our promoter motif analysis does indicate
331 the presence of E-boxes in *BMAL2* but this presents a circular argument and
332 further work on the regulation and evolution of *BMAL2* function is required.

333 While we cannot differentiate between an internal or external coincidence
334 model of photoperiodic time measurement in this study, generally the concept
335 of a photoperiodic coincidence timer predicts that on short photoperiods,
336 repressor activity would dominate in the late night. In line with this we show
337 that long-duration melatonin signals elicit repressor gene transcription in the
338 late night, timed approximately 12h after dark onset/rise of melatonin (ZT20
339 SP). Impressively, these repressors are directly implicated in the negative
340 regulation of LP ZT4 induced genes (Supplementary Fig. 4). Amongst these,
341 we show the circadian repressor *DEC1* ⁵⁴ blocks induction, by *BMAL2*, of
342 *EYA3*. Therefore, *DEC1* and *BMAL2* act as a circadian flip-flop switch for

343 photoperiodic time measurement (Fig. 6). It remains unclear whether DEC-
344 mediated repression is via a direct action on E-box sites occupied by BMAL2
345 or indirect, leading to modification of a co-activator complex. The discovery of
346 transcriptional repressors in the latter half of the night on SP contrasts with
347 previously described acute and photoperiod-independent induction of *CRY1*
348 by melatonin onset ^{17,36,45,47}. However, constant light and therefore *CRY1*
349 repression seems to induce the late-night repressor genes, suggesting that
350 these are direct targets of *CRY1*-mediated repression in the early to mid
351 nocturnal phase. This observation along with altered phasing by photoperiod
352 of the *CRY1* protein stability regulator *FBXL21* ^{48,49} indicate that the dynamics
353 of protein degradation of *CRY1* could play a role in discriminating melatonin
354 signal duration.

355 Our study reveals a progressive increase in H3K4me3 marks at transcription
356 start sites of seasonally expressed genes, especially in long photoperiods (Fig.
357 1d). Furthermore, these long photoperiod induced genes are more likely to
358 have multiple transcription start sites marked with H3K4me3 (Fig. 1e,
359 Supplementary Fig. 1g). *EYA3* is a particular example of this showing
360 seasonal regulation of only one out of two transcription start sites, presumably
361 seasonally modulating the transcription of *EYA3* via BMAL2. On transfer to
362 long photoperiods the *EYA3* and *TSHβ* locus show a progressive increase
363 over a number of weeks in H3K4me3 marks matching the increase in
364 expression (Fig. 2c, d). Our earlier work shows that at the individual cell level
365 the transition between winter and summer physiology is a binary, all-or-
366 nothing phenomenon ^{29,59}. Integrating these two findings, we suggest that
367 individual thyrotroph cells of the PT exhibit a distribution of critical day length
368 requirements/sensitivity for circadian triggering of the summer physiology
369 leading to a binary switch in cell phenotype, which in a whole tissue assay
370 would appear as a progressive change in epigenetic status.

371 We therefore envisage a photoperiodic time measurement model in which a
372 melatonin-regulated circadian-based interval timer interacts with the
373 underlying cellular chromatin state, rhythmically recapitulating the final
374 developmental stages of a thyrotroph endocrine cell in response to long days,
375 leading to an adaptive summer-like physiological state. Our data do indicate

376 morphological changes in another PT cell type, the FS cell, however these
377 cells lack melatonin receptors^{60,61} therefore a role in a coincidence timer is
378 unclear. Defining how a flip-flop circadian timer (Fig. 6) interacts with the
379 chromatin state at the level of the single PT cell remains a future challenge.

380 In summary, the use of photoperiod to synchronise life history cycles in a
381 variable environment is an ancestral feature observed in a large majority of
382 species. Even amongst long day and short day breeders the EYA3-TSH
383 circuitry behaves similarly, demonstrating that although the downstream
384 reproductive responses to photoperiod are altered the mechanism of
385 photoperiodic time measurement is shared^{9,13}. The EYA3-TSH circuitry is
386 conserved amongst vertebrates^{9,13,16,21}, as is the use of a
387 circadian/coincidence based system for photoperiodic time measurement^{2,4-7}.
388 Here, we have defined how photoperiodic changes in EYA3/TSH expression
389 stem from a molecular circadian coincidence timer mechanism. We expect
390 this model to be widely applicable across the vertebrate lineage.

391 **Methods**

392 *Animals & experimental design*

393 All animal experiments were undertaken in accordance with the Home Office
394 Animals (Scientific Procedures) Act (1986), UK, under a Project License held
395 by A.S.I.L. Scottish blackface castrate males were housed in artificial light
396 dark cycles, either 8:16 h light/dark cycle for short photoperiod (SP) or 16:8 h
397 light/dark cycle for long photoperiod (LP).

398 Two separate photoperiod controlled studies were undertaken; 1. The
399 experiment presented in Fig. 1b (seasonal comparison) & Fig. 4a (diurnal
400 comparison at day 28), and, 2. The experiment presented in Fig. 5a
401 (melatonin implant study). Animals were blood sampled throughout the study
402 and terminally sampled at the indicated time-points (Figure 1b, Figure 4a,
403 Figure 5a). The seasonal experiment was designed to take into account the
404 effects of a photoperiodic switch from SP (SP day 84) to LP and the
405 progressive seasonal changes (LP day 1, 7, 28 and 112), followed by return to
406 SP (SP day 1, 7, 28). Animals were terminally sampled at ZT4 at all time-
407 points. The diurnal comparison was conducted on day 28 animals from this
408 study, they were sampled across the day at 4 hourly intervals for 24 hours.
409 The melatonin implant study was a separate experiment on pre-conditioned
410 LP animals (8 weeks).

411 All animals were killed by an overdose of barbiturate (Euthatal; Rhone
412 Merieux, Essex, UK) administered intravenously. Hypothalamic blocks with
413 the *pars tuberalis* (PT) and pituitary attached were collected for
414 immunohistochemistry (n=3 per group), electron microscopy (n=3 per group),
415 transcriptomics (n=3 per group), insitu-hybridization (n=4 per group) and
416 epigenomics (n=2 per group). From the omic analyses the PT was dissected
417 to minimise inclusion of transition zone and median eminence. The PT
418 samples were snap frozen on dry ice and stored at -80C.

419 *Hormone assays*

420 Ovine prolactin (oPRL) was measured as in our previous study ²⁹ for 28
421 animals during the seasonal experiment (Fig. 1b). In brief, a competitive

422 ELISA using purified oPRL (ovine prolactin NIDDK-oPRL-21; AFP10692C;
423 from Dr. A Parlow, NHPP, Harbor-UCLA Torrance CA, USA) and a highly
424 specific rabbit anti-ovine prolactin (ASM-R50, produced by ASM) were used.
425 Plates were read at 450nm. The Coefficient of Variation for the assay on
426 control plasma samples was <10%.

427 Ovine melatonin was measured by radioimmunoassay as previously
428 described ⁴⁷ for animals in the melatonin implant study (Fig. 5a, n=6 per
429 timepoint). In brief, using a rabbit antimelatonin antiserum (PF1288; P.A.R.I.S.,
430 Paris, France) and 2-Iodomelatonin (NEX236050UC; PerkinElmer, Boston,
431 Massachusetts) as tracer RIA was performed. All samples were assayed in a
432 single assay with an intra-assay coefficient of variation of 5% and a sensitivity
433 of 5 pg/mL.

434 *Immunohistochemistry*

435 Tissues (n=3 per group) were immersed in Bouin's fixative for 8 hours,
436 transferred to 70% ethanol, then dehydrated and embedded in paraffin wax.
437 Sagittal sheep brain sections were cut from paraffin embedded tissue at 5 µM,
438 floated onto Superfrost Plus slides (J1800 AMNZ, Thermo scientific), dried at
439 50°C overnight, then dewaxed and rehydrated. Triple immunoflourescence for
440 TSHb, CHGA and EYA3, and the double immunoflourescence for DEC1 / α GSU
441 was performed as in our previous study ²⁹.

442 DEC1 primary antibody (CW27, gift from Prof. Adrian L Harris, Weatherall
443 Institute of Molecular Medicine, John Radcliffe Hospital, Oxford) ⁶² was used
444 at 1:2000. 1:1000 diluted horse radish peroxidase conjugated chicken anti-
445 rabbit IgG antibody was used as a secondary antibody (PI-1000, Vector
446 Laboratories). TSA Plus Cyanine 5 (NEL763001KT, Perkin Elmer) was used
447 to visualize. α GSU immunofluorescence was used at 1:2000 diluted, ASM-
448 HRSU, R20) and treated with TSA Plus Fluorescein (NEL741001KT, Perkin
449 Elmer). Nuclei were stained by Hoechst 33258 (ab228550, abcam) and cover
450 glasses were mounted by VectaMount AQ (H-5501, Vector Laboratories).
451 Images were collected on a Zeiss Axioimager.D2 upright microscope using a
452 40x / 0.7 Plan neofluar objective and captured using a Coolsnap HQ2 camera

453 (Photometrics) through Micromanager Software v1.4.23. Images were then
454 processed using Fiji ImageJ (<http://imagej.net/Fiji/Downloads>).

455 *In Situ Hybridization (ISH) and Quantification of Signal*

456 The OaTSH β plasmid (XM_004002368.2) was kindly provided by David
457 Hazlerigg. The OaEya3 plasmid (NM_001161733.1) was cloned as previously
458 described ²². The OaCHGA, OaDEC1, OaREVERB-alpha, CHRONO and
459 OaBMAL2 were cloned as 1,948-1,970 of XM_004017959.4, 407-767 of
460 NM_001129741.1, 1,012-1,411 of NM_001131029.1, 83-532 of
461 XM_027974329.1, and 1,518-1,906 of XM_027965976.1, respectively.

462 Frozen coronal ovine hypothalamic blocks (n=4 per group) for in-situ
463 hybridization were cut into 16 μ m sections using a cryostat (CM3050s Leica
464 Microsystems, Ltd., Milton Keynes, UK), and thaw mounted onto poly-l-lysine
465 coated slides (VWR International, Lutterworth, UK). Radiolabelled cRNA
466 riboprobes were prepared by plasmid linearization and transcribed using P33
467 α -UTP (Perkin-Elmer). Fixed sections were hybridized overnight at 60°C with
468 5 x 10⁵ cpm of probe per slide. Hybridization signals were visualised on
469 autoradiographic film (Kodak Biomax MR Films, Kodak, USA) after one week
470 exposure at -80°C. Signal intensity was quantified by densitometry analysis of
471 autoradiographs using the image-Pro Plus 6.0 software (Media Cybernetics,
472 Inc., Marlow, UK).

473 *Tissue processing and electron microscopy (EM)*

474 Hypothalamo-pituitary tissue blocks were fixed by immersion in 3%
475 paraformaldehyde/0.05% paraformaldehyde in 0.1M phosphate buffer (pH
476 7.2) for 24 hours at room temperature and transferred to a 1:10 dilution of the
477 fixative in 0.1M phosphate buffer for storage at 4°C before processing (n=3
478 per group). Using a scalpel blade, areas from the medial PT and median
479 eminence were cut into 0.5mm³ pieces which were then stained with osmium
480 (1% in 0.1M phosphate buffer), uranyl acetate (2% w/v in distilled water),
481 dehydrated through increasing concentration of ethanol (70 to 100%),
482 followed by 100% acetone and embedded in Spurr's resin (TAAB laboratory
483 equipment, Aldermarston, UK). Ultrathin sections (50-80 nm) were prepared

484 using a Reichart-Jung Ultracut ultramicrotome and mounted on nickel grids
485 (Agar Scientific Ltd., Stanstead, UK). Sections were then counterstained with
486 lead citrate and uranyl acetate and examined on a JOEL 1010 transmission
487 electron microscope (JOEL USA Inc., Peabody, MA, USA). Sections from 3
488 animals per group were examined.

489 For analysis of PT cell morphology, twenty micrographs per animal (n=3
490 sheep per group) of individual PT cells were taken at a magnification of x
491 5,000. Negatives were scanned into Adobe Photoshop CS2 (Adobe Corp.,
492 San Jose, CA, USA) and analysed using Axiovision version 4.5 (Zeiss,
493 Oberkochen, Germany) image analysis software. The analyst was blind to the
494 sample code. For measurement of the cell and nuclear areas, margins were
495 drawn around the cell or nucleus respectively and the area was calculated.
496 All morphometric values represent the mean \pm SEM (n=3 sheep per group).
497 Means were compared by one way analysis of variance (ANOVA) with post
498 hoc analysis by the Bonferroni test. P<0.05 was considered statistically
499 different.

500 *RNA-seq*

501 RNA was extracted from the pars tuberalis from the seasonal experiment
502 (including the diurnal samples)(Fig1b & Fig. 4a) using Qiagen's TissueLyser II
503 and RNeasy tissue kit (n=3 per group). The quality of the extracted RNA was
504 assessed using the Agilent 2100 Bioanalyser; all RNA integrity numbers
505 (RINs) were above 8, indicating that good quality RNA had been extracted.
506 Poly-A selection was used.

507 RNA was prepared with TruSeq Stranded mRNA Sample Preparation Guide,
508 (15031047 Rev. E, Oct 2013) and sequenced on HiSeq 2500 with 125 base
509 pair paired-end reads by Edinburgh Genomics.

510 The FASTQ files were trimmed with TrimGalore v0.4.0 and mapped (TopHat⁶³
511 v2.1.0 and Bowtie⁶⁴ v2.3.5) to the 5th release of the sheep genome
512 (Oar_rambouillet_v1.0; assembly GCA_002742125.1). StringTie⁶⁵ was used
513 to combine RNASeq and IsoSeq full-length transcripts to generate the
514 genome transcript annotation (accessible in GEO, GSE144677). On average

515 90% (sdev: 8.46) of paired reads generated were mapped to the genome and
516 73% (stdev: 0.03) of these were assignable to genes using featureCount ⁶⁶
517 (Subread v1.6.3).

518 All sequence data have been submitted to SRA under the BioProject
519 accession PRJNA391103 and processed data to GEO under GSE144677.

520 A limma-voom ⁶⁷ analysis pipeline was used to determine the statistical
521 significance of differential expressed genes. Voom was used to generate
522 normalized precision weighted counts per million (CPM) values which were
523 used in the following regression analyses.

524 *Seasonal comparison*

525 The effect of switching from SP to LP was assessed by comparing SP day 84
526 to LP day 1, 7 and 28, and the effect of switching from LP to SP was
527 assessed by comparing LP day 112 to SP day 1, 7 and 28 (Fig. 1b,
528 Supplementary Data 3). For each gene, we fit a least squared regression
529 model with limma that calculates a single f-test for significance across all
530 model coefficients (mitigating type I errors). Time (days) was treated as a
531 categorical independent variable model for all ZT4 observations in LP and SP
532 (photoperiod x day) in limma and which allowed us to extract from the model
533 the fold change and significance for each pairwise contrasts of interest in
534 limma (Supplementary Data 3; Figure 3a,b). Significance was determined by
535 an FDR < 0.05, >0 log2CPM and a >1 log2 absolute fold change.

536 *Diurnal comparison*

537 To test for diurnal changes, samples collected at day 28 in LP and SP at a 4hr
538 time resolution were used (n=3 per group, 7 time-points, Fig. 4a). We used a
539 polynomial regression model approach similar to that of maSigPro⁶⁸. Least
540 squared regression models were then fitted with orthogonal polynomials up to
541 the 5th order for time in each photoperiod to identify significantly changing
542 genes. To test for rapid single time-point changes in gene expression a
543 categorical regression model was also fitted to this dataset. Diurnal genes that
544 were significantly changing across time were identified as FDR significance
545 <0.05, log2CPM > 0 and absolute log2 fold change > 1 (Supplementary Data

546 6; Figure 4b,c,d). FDR was calculated throughout using the Benjamini &
547 Hochberg method. Gene expression changes between photoperiods were
548 evaluated by fitting a photoperiod x time (orthogonal polynomials up to 5th
549 order) model and extracting the significance and effect size from photoperiod
550 coefficient of the linear model (Supplementary Data 6). In selecting the
551 polynomial we used Akaike information criterion (AIC) to investigate the
552 optimal model selection for expressed genes, balancing model overfitting and
553 underfitting (using the Oshlack and Gordon selectModel implementation in
554 limma). It is not possible to select a single model that is optimal across all
555 genes, however for genes > 0 log2CPM and with an amplitude > 1.5 we found
556 that including orthogonal polynomials up to 5th order was optimal for the most
557 genes in both SP and LP time-series. Again we used the thresholds FDR
558 significance <0.05, log2CPM > 0 and absolute log2 fold change > 1
559 (Supplementary Data 6). MetaCycle⁶⁹ v1.1.0 was used to evaluate gene
560 expression in the 24hr time series for periodicity. JTKCyle⁴¹ and Lomb-
561 Scargle statistics were calculated for an assumed period of 24 hours
562 (Supplementary Data 6). Rayleigh tests for uniformity were performed with the
563 CircStats 0.2-6 package in R. We tested the uniformity of distribution of peak
564 expression times for genes containing each of the core clock motifs (canonical
565 EBOXs (CACGTG), DBOXs (TTA[CT][GA]TAA) and RORE sites
566 (AANTAGGTCA)) within the H3K4me3 marked region proximal (within 500bp)
567 of the TSS.

568 For all gene cohorts described enrichment analysis of GO terms and
569 pathways was conducted using both consensusPathDB⁷⁰ and TopGO⁷¹ 3.1.0.
570 Significant terms extracted by a FDR < 0.05 from a fishers exact test. The
571 weight01 algorithm was used for GO term weighting in TopGO. Where gene
572 annotation did not yet exist for novel and unannotated transcripts OrthoMCL⁷²
573 v5 was used to predict orthology from protein sequences and annotation,
574 which were then used to transfer annotation from cow, human, mouse and rat
575 genes. Protein sequences were predicted from novel transcripts using
576 TransDecoder v5.3.0 guided by Uniprot⁷³ and Pfam⁷⁴ best hits to rank coding
577 frames.

578 We clustered SP and LP time-series profiles using Partitioning Around
579 Medoids (PAM) (Fig. 4g) with the cluster 2.1.0 package in R. Day 28, 24 hour,
580 time-series were mean normalized and scaled and PAM clustered with
581 Euclidian distance. The Davies Bouldin index was used to evaluate the
582 optimum number of clusters (k=15 SP and k=9 LP). Motif enrichment of genes
583 clusters was evaluated using fishers two-way exact test against all PT
584 expressing genes as the background. Motifs we identified within H3K4me3
585 marked regions within 500bp of a candidate TSS assigned to a gene.

586 *ChIP-seq*

587 The method used for ChIP-seq was adapted from an ultra low cell number
588 native ChIP method ⁷⁵. In brief, nuclei were isolated from whole PT tissue
589 (n=2 per group) with a dounce homogenizer and sigma nuclear isolation
590 buffer. Mnase digestion was optimized to give the best discrimination
591 between mono, di and tri histones. Immunoprecipitation was performed with
592 protein A and G beads (Invitrogen). Importantly the beads were pre-incubated
593 with the H3K4me3 antibody (active motif) to reduce background noise.
594 Stringent washing with salt buffers was also used to reduce the background
595 noise. The bound chromatin was elute and extracted using a phenol
596 chloroform method. Ampure bead purification was used to clean up the
597 samples. The qubit and tapestation were used to quantify, a minimum amount
598 of 5ng was required for the library preparation. The Manchester genomic
599 facility prepared the ChIP-seq libraries and sequenced them according to the
600 standard illumina protocol.

601 Massive parallel sequencing were performed by Illumina HiSeq4000 with 75
602 bp paired-end and converted fastqs by bcl2fastq (ver 2.17.1.14). Fastqs were
603 trimmed by trimmomatic (ver 0.36) ⁷⁶ with the following parameters,
604 ILLUMINACLIP: TruSeq3-PE-2.fa:2:30:10 SLIDINGWINDOW:4:20
605 MINLEN:35, aligned to the sheep genome (Oar_rambouillet_v1.0) by BWA
606 MEM (ver 0.7.17) ⁷⁷ with the default parameter and then converted to BAM
607 and sorted by samtools (ver 0.1.19). Peak calling were carried out by MACS2
608 (ver 2.1.0) ⁷⁸ with following parameters, --format BAMPE --gsize 2.81e9 --
609 keep-dup 1 --broad --broad-cutoff 0.1 --bdg --SPMR --qvalue 0.05.

610 Read coverages of peaks were calculated by SICER (ver 1.1)⁷⁹ with following
611 parameters; window size=200, gap length=200, fdr=0.01. BED files of
612 replicate samples were merged in order to perform SICER analysis which
613 does not allow replicates. Peaks called by SICER were annotated by HOMER
614 (ver 4.10.3)⁸⁰ with default parameters. H3K4me3 peaks identified by SICER
615 were validated by monitoring the distributions on the sheep genome. By
616 HOMER annotation, each peak was described as promoter-TSS (1000 bp
617 from TSSs), exon, intron, TTS, intergenic and the distributions of H3K4me3
618 peaks were closely resembling to the previous reports^{33,34} (Supplementary
619 Fig. 6a). Furthermore, H3K4me3 peaks were well-associated with CpG
620 islands (CGIs) on the sheep genome as described in the previous study
621 (Supplementary Fig. 6b)³⁵. We use a standard definition of CpG islands⁸¹;
622 nucleotides regions with > 50% GC content, extending to > 200 bp and with
623 an observed vs expected CpG ratio >6.5, and detected them using
624 CgiHunterLight 1.0 on Oar_rambouillet_v1.0 (assembly GCA_002742125.1).
625 H3K4me3 peaks of each sampling day were shuffled by bedtools shuffle (ver
626 2.27.1)⁸² with -noOverlapping as negative controls. For correlation analysis
627 with RNA expression, ChIP read counts of peaks overlapped in ± 200 bp from
628 TSSs were used. A workflow diagram can be found in Supplementary Fig. 7.

629 /ISO-seq

630 For gene annotation, five tissue samples were sequenced over two
631 experimental runs using PacBio Iso-Seq. In the first run PT and PD samples
632 were sequenced from an RNA pool of SP and LP Scottish blackface sheep
633 (N=1) and a pineal from a commercial mule sheep from Manchester, UK. This
634 RNA was sent to GATC Biotech (Konstanz, Germany) for cDNA library
635 preparation using their in-house method with mRNA 5' cap and poly(A) tail
636 selections and sequencing on a PacBio RSII system. GATC made full length
637 normalized RNA libraries.size selected for <2kb, 2kb-4kb, >4kb. sequenced
638 across 75 PacBio RS II SMRT cells [[SRX7688275](#)]. In a second run, PT from
639 a pool of sheep in LP, and SP (n=3) were sequenced. RNA was extracted
640 using RNeasy Mini Kit (Qiagen) with on-column Dnase digestion. A full-length
641 cDNA library was constructed for each sample using the TeloPrime Full-
642 Length cDNA Amplification Kit V1 (Lexogen) and amplified using PrimeSTAR

643 GXL DNA Polymerase (Takara Bio) with 22 PCR cycles of 98 °C denaturation
644 for 10 seconds, 60 °C annealing for 15 seconds, and 68 °C extension for 10
645 minutes. PacBio SMRTbell libraries were prepared using SMRTbell Template
646 Prep Kit 1.0 and each library was sequenced on two SMRT Cells v2 LR using
647 20-hour movies on a Sequel platform at the IMB Sequencing Facility
648 (University of Queensland, [\[SRX7688271\]](#)). All Iso-Seq data was first
649 processed using software IsoSeq v3.1 to obtain full-length non-concatemer
650 reads with at least 3 full sequencing passes, which were then mapped to the
651 sheep reference genome GCA_002742125.1 using GMAP version 2018-05-
652 30. TAMA Collapse from the TAMA tool kit ⁸³ was used to generate unique
653 gene and transcript models, which were further merged with RNAseq-based
654 annotation data using TAMA Merge to incorporate any transcript models that
655 were identified by RNAseq but not Iso-Seq. Functional annotation of
656 transcripts was carried out using Trinotate (v3.1.1).

657 Where multiple transcripts were present for an expressed gene, with more
658 than one transcription start sites (TSS) candidate, the active proximal
659 promoter regions were inferred by selecting contiguous H3K4me3 marked
660 regions within 100bp of a TSS.

661 CAGE-seq

662 We applied cap analysis gene expression (CAGE) to identify the location and
663 relative expression of TSS regions of the PT across both LP and SP. When
664 combined with IsoSeq and RNASeq derived transcript annotation this
665 provided a comprehensive identification of TSS in the genome which allowed
666 us to more accurately apply DNA binding motif analysis to promoter regions.
667 Libraries were prepared according to Hazuki *et. al* ³² and sequenced on an
668 Illumina HiSeq 2500 using V4 chemistry on a 50 cycle Single end sequencing
669 run. We sequenced archived RNA samples from the PT in both SP and LP
670 (ZT4, week 12) ²⁹. We also sequenced RNA from PD (both SP and LP), and
671 Pineal for comparison as outgroups. Reads were trimmed using fastx toolkit
672 0.0.14 and cutadapt 1.4. Reads were mapped using BWA 0.7.17 to the 5th
673 release of the sheep genome (Oar_rambouillet_v1.0; assembly
674 GCA_002742125.1). CAGER 1.26.0 was used for processing and cluster

675 analysis of TSS (Supplementary Data 4). We filtered reads for a mapping
676 quality > 30 and sequencing quality > 20. Tag counts were normalised using
677 the power law method with an alpha of 1.12 and T of 10^6 (determined by
678 plotting the reverse cumulatives of PT samples). We clustering TSS with >1
679 TPM together using the distclu methods allowing a max distance between
680 TSS of 20 nucleotides.

681

682 *Transcription factor binding site analysis*

683 Transcription Factor binding motifs were identified using the FIMO tool from
684 MEME v4.11.4 with a p-value threshold of $<1 \times 10^{-7}$. for Jasper 2018 core
685 vertebrate database. Fishers one-way exact tests for enrichment were used to
686 identify the significance of motif enrichment within active promoter regions of a
687 gene cohort compared to a background of all PT expressed genes (> 0 CPM).
688 Fishers two-way exact tests were applied to evaluate enrichment and
689 depletion of motifs within active proximal promoter regions of genes with the
690 use of SP and LP H3K4me3 marked regions within 500bp of candidate TSSs.

691 *Protein-protein interaction networks*

692 Using experimentaly evidenced protein-protein interaction (PPI) annotation
693 from the STRING ⁵⁰ v10 database for cow, sheep, rat, mouse and human we
694 integrated protein interactions in Cytoscape ⁸⁴ with significantly changing
695 genes in the ZT 4 SP vs ZT20 LP from the 24 hr categorical contrast, which is
696 12 hrs from dark/melatonin onset (Supplementary Data 6 & Supplementary
697 Figure 4). A threshold of >0.4 for confidence score in experimental evidence
698 and a combined score of > 0.7 was applied, and orphaned proteins removed
699 from the network. The significance of enrichment of PPI repressor connected
700 genes within up-regulated vs down-regulated genes was evaluated using
701 fishers two-way exact tests.

702 *Cloning and constructs*

703 Expression plasmids: PCR fragments of the expected sizes were extracted
704 using a gel extraction kit (Qiagen) and cloned in pGEM-T easy vector

705 (Promega); Four to six positive clones were sequenced (MWG, United
706 Kingdom). To generate expression constructs, a second round of PCR was
707 performed using primers flanked by adequate restriction sites and the pGEM-
708 T clone as template. PCR fragments were extracted as described above,
709 digested by the adequate restriction enzymes, purified with a PCR purification
710 kit (Qiagen) and cloned in the expression vector backbone (pCS2-HIS). In
711 order to generate the mutant expression plasmids for BMAL2 we used the
712 QuikChange Lightning Multi Site-Directed Mutagenesis Kit (210515, Agilent).
713 The bHLH mutant was generated by converting an arginine to alanine
714 (OaBMAL2_R88A) based on a mouse mutagenesis study on BMAL1³⁷. The
715 PAS-B mutant was made by converting a phenylalanine to arginine, and a
716 valine to arginine (OaBMAL2_F427R_V439R). Based on a on a mouse
717 mutagenesis study on BMAL1⁴⁰.

718 Sanger sequencing of clones are available in Genbank for BMAL2 cds
719 constructs (Genbank: [\[MT001920\]](#)), DEC1 cds constructs (Genbank:
720 [\[MT019539\]](#)), DEC2 cds constructs (Genbank: [\[MT019540\]](#)), PAS-B-mutated
721 BMAL2 cds constructs (Genbank: [\[MT019541\]](#)), bHLH-mutated BMAL2 cds
722 constructs (Genbank: [\[MT019542\]](#)),

723 Promoter reporter constructs: a strategy identical to that described above was
724 applied and fragments were cloned into the pGL4 basic backbone (Promega)
725 digested with the appropriate restriction enzymes. Sequencing was performed
726 to check accuracy of all re-amplified cloned fragments. EYA3 generic and
727 seasonal promoter construct sequences are available on genebank
728 ([\[MT001921\]](#) and [\[MT001924\]](#) respectively).

729 *Cell culture, transfection and luciferase reporter assays*

730 The procedure was as previously reported ²². In brief, COS-7 cells were
731 grown in Dulbecco's modified eagle's medium supplemented with 10% fetal
732 bovin serum, 1% penicillin/streptomycin at 5% CO₂ and 37°C. Cells were
733 plated in 24-well plates at a density of 4x10⁴ cells per ml and incubated for 24
734 hours prior to transfection. Transfection was performed using Genejuice
735 (Novagen) and the concentration was optimised to transfet the greatest
736 number of cells without compromising cell survival, this was assessed using a

737 luciferase positive control pGL3 containing SV40 (Promega) and trypan blue
738 staining. We recorded a 90% cell survival and a high transfection efficiency.
739 The EYA3 promoter constructs were used at 50ng per well, as in a previous
740 study ²². The expression plasmids were used at different doses based on a
741 previous study and optimization of the assay: TEF = 12.5ng, DEC1 = 25ng,
742 CLOCK, BMAL1, BMAL2 and mutant BMAL2 were all used at 50ng, unless
743 otherwise stated. The total transfected DNA amount was set to an equal
744 amount between all conditions by addition of the corresponding empty vector.
745 The luciferase assays were performed 48 hours after transfection using the
746 luciferase assay kit (Promega) and the Glomax luminometer (Promega).
747 The total protein per well, assessed by Bradford assay was used to normalize
748 the values to total protein content (a proxy for cell number). All data (in
749 Relative Luminescence Units, RLU) represent fold induction once normalized
750 to total protein content and relative to an inert control transfection. Each
751 experiment contained 4 replicate wells and was repeated 4 times giving
752 similar results. An one-way ANOVA using Tukey's multiple comparisons test
753 was performed for each separate experiment conducted in Graphpad prism
754 7.05. Representative plots (n=4) are shown.

755 *Data availability statement*

756 All sequence data supporting the findings of this study have been deposited in
757 the Sequence Read Archive (SRA) under the BioProject accession
758 [[PRJNA391103](#)] and processed data to GEO under [[GSE144677](#)]. Chip-seq
759 raw fastq is available in SRA [[SRP110487](#)] and processed bigWig data for in
760 GEO [[GSE144515](#)]. Additionally, we have made the bigWig data for
761 rambouillet 1.0 genome [[GCF_002742125.1](#)] available as a track hub for use
762 with NCBI browser at [https://data.cyverse.org/dav-
763 anon/iplant/home/mhindle/hub.txt](https://data.cyverse.org/dav-anon/iplant/home/mhindle/hub.txt) that can be loaded in NCBI Genome Data
764 Viewer. CAGE raw data is available in SRA [[SRP110487](#)] and as BigWig
765 annotations in the public trackhub. Source data for Figure 1b, Figure 1c,
766 Figure 3c, Figure 3d, Figure 3e, Figure 3f, Figure 5c, Figure 5d, Figure 5e,
767 Figure 5f and Figure 5h are provided with the paper.

768 *Code availability statement*

769 Code used is available from the authors on request.

770 **References**

- 771 1. Bünning, E. Die endogene Tagesperiodik als Grundlage der
772 photoperiodischen Reaktion. *Ber Dtsch Bot Ges* **54**, 590–608 (1936).
- 773 2. Pittendrigh, C. S. & Minis, D. H. The entrainment of circadian
774 oscillations by light and their role as photoperiodic clocks. *Am. Nat.* **98**,
775 261–299 (1964).
- 776 3. Nanda, K. K. & Hamner, K. . Studies on the nature of the endogenous
777 rhythm affecting photoperiodic response of Biloxi soybean. *Bot. Gaz.*
778 **120**, 14–28 (1958).
- 779 4. Follett, B. K., Mattocks, P. W. & Farner, D. S. Circadian function in the
780 photoperiodic induction of gonadotropin secretion in the white-crowned
781 sparrow, *Zonotrichia leucophrys gambelii*. *Proc. Natl. Acad. Sci. U. S. A.*
782 **71**, 1666–9 (1974).
- 783 5. Goldman, B. D. Mammalian photoperiodic system: formal properties
784 and neuroendocrine mechanisms of photoperiodic time measurement. *J.*
785 *Biol. Rhythms* **16**, 283–301 (2001).
- 786 6. Pittendrigh, C. S., Elliott, J. & Takamura, T. The Circadian Component
787 in Photoperiodic Induction. in 26–47 (Wiley-Blackwell, 2008).
788 doi:10.1002/9780470720851.ch4
- 789 7. Ikegami, K. & Yoshimura, T. Circadian clocks and the measurement of
790 daylength in seasonal reproduction. *Mol. Cell. Endocrinol.* **349**, 76–81
791 (2012).
- 792 8. Bartness, T. J., Powers, J. B., Hastings, M. H., Bittman, E. L. &
793 Goldman, B. D. The timed infusion paradigm for melatonin delivery:
794 what has it taught us about the melatonin signal, its reception, and the
795 photoperiodic control of seasonal responses? *J. Pineal Res.* **15**, 161–90
796 (1993).
- 797 9. Wood, S. & Loudon, A. Clocks for all seasons: unwinding the roles and
798 mechanisms of circadian and interval timers in the hypothalamus and

799 pituitary. *J. Endocrinol.* **222**, R39-59 (2014).

800 10. Woodfill, C. J. I., Wayne, N. L., Moenter, S. M. & Karsch, F. J.
801 Photoperiodic Synchronization of a Circannual Reproductive Rhythm in
802 Sheep□: Identification of Season-Specific Time Cues ' Reproductive
803 Sciences Program and Department of Physiology , University of
804 Michigan. *Biol. Reprod.* **50**, 965–976 (1994).

805 11. Lincoln, G. A. & Ebling, F. J. P. Effect of constant-release implants of
806 melatonin on seasonal cycles in reproduction, prolactin secretion and
807 moulting in rams. *Reproduction* **73**, 241–253 (1985).

808 12. Bittman, E. L., Dempsey, R. J. & Karsch, F. J. Pineal melatonin
809 secretion drives the reproductive response to daylength in the ewe.
810 *Endocrinology* **113**, 2276–83 (1983).

811 13. Dardente, H., Wood, S., Ebling, F. & Sáenz de Miera, C. An integrative
812 view of mammalian seasonal neuroendocrinology. *J. Neuroendocrinol.*
813 **31**, e12729 (2019).

814 14. Lincoln, G. A. Melatonin Entrainment of Circannual Rhythms.
815 *Chronobiol. Int.* **23**, 301–306 (2006).

816 15. Wood, S. & Loudon, A. The pars tuberalis: The site of the circannual
817 clock in mammals? *Gen. Comp. Endocrinol.* **258**, 222–235 (2017).

818 16. West, A. C. & Wood, S. H. Seasonal physiology: making the future a
819 thing of the past. *Curr. Opin. Physiol.* **5**, 1–8 (2018).

820 17. Johnston, J. D. *et al.* Multiple Effects of Melatonin on Rhythmic Clock
821 Gene Expression in the Mammalian Pars Tuberalis. *Endocrinology* **147**,
822 959–965 (2006).

823 18. West, A. *et al.* Npas4 is activated by melatonin, and drives the clock
824 gene Cry1 in the ovine pars tuberalis. *Mol. Endocrinol.* **27**, 979–989
825 (2013).

826 19. Hanon, E. A. *et al.* Ancestral TSH mechanism signals summer in a
827 photoperiodic mammal. *Curr. Biol.* **18**, 1147–52 (2008).

828 20. Nakao, N. *et al.* Thyrotrophin in the pars tuberalis triggers photoperiodic
829 response. *Nature* **452**, 317–22 (2008).

830 21. Nakane, Y. & Yoshimura, T. Universality and diversity in the signal
831 transduction pathway that regulates seasonal reproduction in
832 vertebrates. *Front. Neurosci.* **8**, 115 (2014).

833 22. Dardente, H. *et al.* A molecular switch for photoperiod responsiveness
834 in mammals. *Curr. Biol.* **20**, 2193–8 (2010).

835 23. Masumoto, K. *et al.* Acute Induction of Eya3 by Late-Night Light
836 Stimulation Triggers TSH β Expression in Photoperiodism. *Curr. Biol.* **20**,
837 2199–2206 (2010).

838 24. Dupré, S. M. *et al.* Identification of Eya3 and TAC1 as long-day signals
839 in the sheep pituitary. *Curr. Biol.* **20**, 829–35 (2010).

840 25. Angel, A., Song, J., Dean, C. & Howard, M. A Polycomb-based switch
841 underlying quantitative epigenetic memory. *Nature* **476**, 105–8 (2011).

842 26. Song, J., Irwin, J. & Dean, C. Remembering the prolonged cold of winter.
843 *Curr. Biol.* **23**, R807-11 (2013).

844 27. Satake, A. & Iwasa, Y. A stochastic model of chromatin modification:
845 Cell population coding of winter memory in plants. *J. Theor. Biol.* **302**,
846 6–17 (2012).

847 28. Dardente, H., Hazlerigg, D. G. & Ebling, F. J. P. Thyroid hormone and
848 seasonal rhythmicity. *Front. Endocrinol. (Lausanne)* **5**, 19 (2014).

849 29. Wood, S. H. *et al.* Binary switching of calender cells in the pituitary
850 defines the phase of the circannual cycle in mammals. *Curr. Biol.* **25**,
851 (2015).

852 30. Karsch, F. J., Robinson, J. E., Woodfill, C. J. & Brown, M. B. Circannual
853 cycles of luteinizing hormone and prolactin secretion in ewes during
854 prolonged exposure to a fixed photoperiod: evidence for an endogenous
855 reproductive rhythm. *Biol. Reprod.* **41**, 1034–46 (1989).

856 31. Lincoln, G. A., Clarke, I. J., Hut, R. A. & Hazlerigg, D. G. Characterizing
857 a mammalian circannual pacemaker. *Science* **314**, 1941–4 (2006).

858 32. Takahashi, H., Kato, S., Murata, M. & Carninci, P. CAGE (Cap analysis
859 of gene expression): A protocol for the detection of promoter and
860 transcriptional networks. *Methods Mol. Biol.* **786**, 181–200 (2012).

861 33. Hussey, S. G., Loots, M. T., van der Merwe, K., Mizrahi, E. & Myburg,
862 A. A. Integrated analysis and transcript abundance modelling of
863 H3K4me3 and H3K27me3 in developing secondary xylem. *Sci. Rep.* **7**,
864 3370 (2017).

865 34. Ershov, N. I. *et al.* Consequences of early life stress on genomic
866 landscape of H3K4me3 in prefrontal cortex of adult mice. *BMC*
867 *Genomics* **19**, 93 (2018).

868 35. Rose, N. R. & Klose, R. J. Understanding the relationship between DNA
869 methylation and histone lysine methylation. *Biochim. Biophys. Acta -*
870 *Gene Regul. Mech.* **1839**, 1362–1372 (2014).

871 36. Lincoln, G., Messager, S., Andersson, H. & Hazlerigg, D. Temporal
872 expression of seven clock genes in the suprachiasmatic nucleus and
873 the pars tuberalis of the sheep: evidence for an internal coincidence
874 timer. *Proc. Natl. Acad. Sci. U. S. A.* **99**, 13890–5 (2002).

875 37. Hosoda, H., Motohashi, J., Kato, H., Masushige, S. & Kida, S. A BMAL1
876 mutant with arginine 91 substituted with alanine acts as a dominant
877 negative inhibitor. *Gene* **338**, 235–41 (2004).

878 38. Spiegelman, B. M. & Heinrich, R. Biological Control through Regulated
879 Transcriptional Coactivators. *Cell* **119**, 157–167 (2004).

880 39. Guo, Y., Scheuermann, T. H., Partch, C. L., Tomchick, D. R. & Gardner,
881 K. H. Coiled-coil Coactivators Play a Structural Role Mediating
882 Interactions in Hypoxia-inducible Factor Heterodimerization. *J. Biol.*
883 *Chem.* **290**, 7707–7721 (2015).

884 40. Huang, N. *et al.* Crystal Structure of the Heterodimeric CLOCK:BMAL1

885 41. Transcriptional Activator Complex. *Science* (80-). **337**, 189–194 (2012).

886 41. Hughes, M. E., Hogenesch, J. B. & Kornacker, K. JTK-CYCLE: An
887 efficient nonparametric algorithm for detecting rhythmic components in
888 genome-scale data sets. *J. Biol. Rhythms* **25**, 372–380 (2010).

889 42. Xu, H. *et al.* Cryptochrome 1 regulates the circadian clock through
890 dynamic interactions with the BMAL1 C terminus. *Nat. Struct. Mol. Biol.*
891 **22**, 476–484 (2015).

892 43. Maywood, E. S. *et al.* Translational switching of Cry1 protein expression
893 confers reversible control of circadian behavior in arrhythmic Cry-
894 deficient mice. *Proc. Natl. Acad. Sci.* **115**, E12388–E12397 (2018).

895 44. Patch, C. L., Green, C. B. & Takahashi, J. S. Molecular architecture of
896 the mammalian circadian clock. *Trends Cell Biol.* **24**, 90–99 (2014).

897 45. Dardente, H. *et al.* Melatonin induces Cry1 expression in the pars
898 tuberalis of the rat. *Mol. Brain Res.* **114**, 101–106 (2003).

899 46. Dupré, S. M. *et al.* Identification of melatonin-regulated genes in the
900 ovine pituitary pars tuberalis, a target site for seasonal hormone control.
901 *Endocrinology* **149**, 5527–39 (2008).

902 47. West, A. *et al.* Npas4 is activated by melatonin, and drives the clock
903 gene Cry1 in the ovine pars tuberalis. *Mol. Endocrinol.* (2013).
904 doi:10.1210/me.2012-1366

905 48. Hirano, A. *et al.* FBXL21 Regulates Oscillation of the Circadian Clock
906 through Ubiquitination and Stabilization of Cryptochromes. *Cell* **152**,
907 1106–1118 (2013).

908 49. Dardente, H., Mendoza, J., Fustin, J.-M., Challet, E. & Hazlerigg, D. G.
909 Implication of the F-Box Protein FBXL21 in Circadian Pacemaker
910 Function in Mammals. *PLoS One* **3**, e3530 (2008).

911 50. Szklarczyk, D. *et al.* The STRING database in 2017: quality-controlled
912 protein–protein association networks, made broadly accessible. *Nucleic
913 Acids Res.* **45**, D362–D368 (2017).

914 51. Maywood, E. S. *et al.* The effect of signal frequency on the gonadal
915 response of male Syrian hamsters to programmed melatonin infusions.
916 *J. Neuroendocrinol.* **4**, 37–44 (1992).

917 52. Ebling, F. J., Lincoln, G. A., Wollnik, F. & Anderson, N. Effects of
918 constant darkness and constant light on circadian organization and
919 reproductive responses in the ram. *J. Biol. Rhythms* **3**, 365–84 (1988).

920 53. Staples, L. D., McPhee, S., Kennaway, D. J. & Williams, A. H. The
921 influence of exogenous melatonin on the seasonal patterns of ovulation
922 and oestrus in sheep. *Anim. Reprod. Sci.* **30**, 185–223 (1992).

923 54. Honma, S. *et al.* Dec1 and Dec2 are regulators of the mammalian
924 molecular clock. *Nature* **419**, 841–844 (2002).

925 55. Dardente, H., Fustin, J.-M. & Hazlerigg, D. G. Transcriptional feedback
926 loops in the ovine circadian clock. *Comp. Biochem. Physiol. Part A Mol.*
927 *Integr. Physiol.* **153**, 391–398 (2009).

928 56. Hazlerigg, D., Lomet, D., Lincoln, G. & Dardente, H. Neuroendocrine
929 correlates of the critical day length response in the Soay sheep. *J.*
930 *Neuroendocrinol.* e12631 (2018). doi:10.1111/jne.12631

931 57. Gustafson, C. L. & Partch, C. L. Emerging Models for the Molecular
932 Basis of Mammalian Circadian Timing. *Biochemistry* **54**, 134–149
933 (2015).

934 58. Bunger, M. K. *et al.* Mop3 Is an Essential Component of the Master
935 Circadian Pacemaker in Mammals. *Cell* **103**, 1009–1017 (2000).

936 59. Wood, S. H. How can a binary switch within the pars tuberalis control
937 seasonal timing of reproduction? *J. Endocrinol.* **239**, R13–R25 (2018).

938 60. Klosen, P. *et al.* The mt1 melatonin receptor and RORbeta receptor are
939 co-localized in specific TSH-immunoreactive cells in the pars tuberalis
940 of the rat pituitary. *J. Histochem. Cytochem.* **50**, 1647–57 (2002).

941 61. Dardente, H., Klosen, P., Pévet, P. & Masson-Pévet, M. MT1 melatonin
942 receptor mRNA expressing cells in the pars tuberalis of the European

943 hamster: effect of photoperiod. *J. Neuroendocrinol.* **15**, 778–86 (2003).

944 62. Turley, H. *et al.* The hypoxia-regulated transcription factor DEC1(Stra13,
945 SHARP-2) and its expression in human tissues and tumours. *J. Pathol.*
946 **203**, 808–813 (2004).

947 63. Kim, D. *et al.* TopHat2: accurate alignment of transcriptomes in the
948 presence of insertions, deletions and gene fusions. *Genome Biol.* **14**,
949 R36 (2013).

950 64. Langmead, B. & Salzberg, S. L. Fast gapped-read alignment with
951 Bowtie 2. *Nat. Methods* **9**, 357–359 (2012).

952 65. Pertea, M., Kim, D., Pertea, G. M., Leek, J. T. & Salzberg, S. L.
953 Transcript-level expression analysis of RNA-seq experiments with
954 HISAT, StringTie and Ballgown. *Nat. Protoc.* **11**, 1650–1667 (2016).

955 66. Liao, Y., Smyth, G. K. & Shi, W. FeatureCounts: An efficient general
956 purpose program for assigning sequence reads to genomic features.
957 *Bioinformatics* **30**, 923–930 (2014).

958 67. Law, C. W., Chen, Y., Shi, W. & Smyth, G. K. voom: precision weights
959 unlock linear model analysis tools for RNA-seq read counts. *Genome
960 Biol.* **15**, R29 (2014).

961 68. Nueda, M. J., Tarazona, S. & Conesa, A. Next maSigPro: updating
962 maSigPro bioconductor package for RNA-seq time series.
963 *Bioinformatics* **30**, 2598 (2014).

964 69. Wu, G., Anafi, R. C., Hughes, M. E., Kornacker, K. & Hogenesch, J. B.
965 MetaCycle: An integrated R package to evaluate periodicity in large
966 scale data. *Bioinformatics* **32**, 3351–3353 (2016).

967 70. Kamburov, A., Stelzl, U., Lehrach, H. & Herwig, R. The
968 ConsensusPathDB interaction database: 2013 update. *Nucleic Acids
969 Res.* **41**, D793-800 (2013).

970 71. Alexa, A., Rahnenführer, J. & Lengauer, T. Improved scoring of
971 functional groups from gene expression data by decorrelating GO graph

972 structure. *Bioinformatics* **22**, 1600–1607 (2006).

973 72. Li, L., Stoeckert, C. J. & Roos, D. S. OrthoMCL: Identification of ortholog
974 groups for eukaryotic genomes. *Genome Res.* **13**, 2178–2189 (2003).

975 73. UniProt: a worldwide hub of protein knowledge. *Nucleic Acids Res.* **47**,
976 D506–D515 (2019).

977 74. El-Gebali, S. *et al.* The Pfam protein families database in 2019. *Nucleic
978 Acids Res.* **47**, D427–D432 (2019).

979 75. Brind'Amour, J. *et al.* An ultra-low-input native ChIP-seq protocol for
980 genome-wide profiling of rare cell populations. *Nat. Commun.* **6**, 6033
981 (2015).

982 76. Bolger, A. M., Lohse, M. & Usadel, B. Trimmomatic: a flexible trimmer
983 for Illumina sequence data. *Bioinformatics* **30**, 2114–2120 (2014).

984 77. Li, H. & Durbin, R. Fast and accurate short read alignment with
985 Burrows-Wheeler transform. *Bioinformatics* **25**, 1754–1760 (2009).

986 78. Zhang, Y. *et al.* Model-based Analysis of ChIP-Seq (MACS). *Genome
987 Biol.* **9**, R137 (2008).

988 79. Zang, C. *et al.* A clustering approach for identification of enriched
989 domains from histone modification ChIP-Seq data. *Bioinformatics* **25**,
990 1952–1958 (2009).

991 80. Heinz, S. *et al.* Simple Combinations of Lineage-Determining
992 Transcription Factors Prime cis-Regulatory Elements Required for
993 Macrophage and B Cell Identities. *Mol. Cell* **38**, 576–589 (2010).

994 81. Ioshikhes, I. P. & Zhang, M. Q. Large-scale human promoter mapping
995 using CpG islands. *Nat. Genet.* **26**, 61–63 (2000).

996 82. Quinlan, A. R. & Hall, I. M. BEDTools: a flexible suite of utilities for
997 comparing genomic features. *Bioinformatics* **26**, 841–842 (2010).

998 83. Kuo, R. I., Cheng, Y., Smith, J., Archibald, A. L. & Burt, D. W.
999 Illuminating the dark side of the human transcriptome with TAMA Iso-

1000 Seq analysis. *bioRxiv* 780015 (2019). doi:10.1101/780015

1001 84. Shannon, P. *et al.* Cytoscape: A software Environment for integrated
1002 models of biomolecular interaction networks. *Genome Res.* **13**, 2498–
1003 2504 (2003).

1004

1005 **Acknowledgements**

1006 The authors thank Joan Docherty and the staff at the Marshall Building, Roslin,
1007 Edinburgh for expert care of their research animals. Past members of the
1008 Manchester/Edinburgh team have made contributions to discussions and
1009 offered advice, including Sandrine Dupre, and Alex West. We thank David
1010 Hazlerigg, Carrie Partch and Jean Michel Fustin for their critical review of
1011 earlier drafts of this work. The work was supported by grants from the
1012 Biotechnology and Biological Sciences Research Council UK (BB/N015584/1,
1013 BB/N015347/1, BBP013759/1) and a Human Sciences Frontier Programme
1014 Grant RGP0030/2015 Evolution of Seasonal Timers awarded to ASIL and
1015 DWB. ASIL acknowledges the support of the Wellcome Trust, Grant
1016 107851/Z/15/Z

1017

1018 **Author contributions**

1019 **SHW** - designed the experiments, collected samples, performed RNA
1020 preparation, chromatin immunoprecipitation preparation, luciferase reporter
1021 assays, cloning and mutagenesis, analysed/interpreted data, prepared the
1022 manuscript and figures. **MH** – Bioinformatic analysis, data analysis and
1023 submission, sequencing, prolactin assay, figure preparation and revised the
1024 manuscript. **YM** - Bioinformatic analysis, immunohistochemistry, luciferase
1025 reporter assays, cloning and mutagenesis, figure preparation and revised
1026 manuscript. **YC** – ISO-seq and bioinformatic analysis **KM** –
1027 immunohistochemistry and analysis. **HC** – performed EM and analysis,
1028 revised manuscript. **BRCS** - collected samples and performed the in situ
1029 hybridization, luciferase reporter assays, cloning and mutagenesis. **NB** –
1030 collected samples and provided lab support. **JM** - developed the novel
1031 prolactin assay and prepared antibodies. **ASM** - collected samples, designed
1032 experiments, developed the prolactin assay, and revised the manuscript. **SM** -
1033 collected samples, designed experiments, prolactin assay, and revised
1034 manuscript. **DWB** - designed experiments, bioinformatics analysis, and
1035 revised the manuscript. **ASIL** – conceived the study, designed experiments,
1036 collected samples, analysed/interpreted data, and prepared the manuscript.

1037

1038 **Competing interests**

1039 The authors have no competing interests to declare.

1040

1041 **Figure legends**

1042 **Fig. 1:** Photoperiod dependent epigenetic regulation of transcription in the
1043 *Pars tuberalis*

1044 a. Current model for the mammalian photoperiodic circuitry.

1045 b. Prolactin concentrations during the experiment (black), n = 28
1046 biologically independent animals per time-point. Error bars represent the
1047 SEM. Grey line: number of hours of light the animals received in 24 hours.
1048 Red arrows show terminal sampling points (ZT4), with the exception of day
1049 28 where animals were collected across the day at 4 hour intervals.

1050 c. EM images of PT thyrotrophs and PD somatotrophs at LP day 28 and
1051 SP day 28. Dense chromatin in the nucleus is false coloured in purple.
1052 Black scale bars = 2um.

1053 d. Histogram revealing frequency distributions of Pearson correlation
1054 coefficients between RNA expression (\log_2 CPM) and H3K4me3 peak read
1055 counts ± 200 bp from TSSs (\log_2 read counts). Red bars are seasonally
1056 expressed genes (\log_2 fold change ≥ 1 or ≤ -1 and adjusted p value < 0.05
1057 of short photoperiod (SP) day 84 vs long photoperiod (LP) day 1, 7, 28 and
1058 LPday112 vs SPday1, 7, 28 differentially expressed genes (DEGs)=480)
1059 and black bars are non-seasonally expressed genes (\log_2 fold change \leq
1060 0.1 and ≥ -0.1 from the same comparisons, (genes=218)).

1061 e. Prevalence of multiple (>1) TSS's in LP day28 up-regulated DEGs (solid
1062 red), SP day 28 up-regulated DEGs (solid blue) and all PT expressed
1063 genes as the background (solid black) as a percentage of the uppermost
1064 expressed genes (i.e. increasing thresholds for the upper quantile of gene
1065 expression). Log2CPM values for upper quantiles on upper x-axis. Dashed

1066 lines indicate the proportion of gene in the cohorts with multiple H3K4me3
1067 (>1) marked TSS.

1068 f. Over-represented motifs LP day 28 up and down-regulated genes,
1069 compared to SP day 28. The percentage of H3K3me3 marked TSS (+/-
1070 100bp) containing a specific motif is given. The black triangles represents
1071 the motif abundance in all the genes expressed (>0 CPM) in the PT and
1072 the percentage of marked with H3k4me3 in LP (x-axis) or SP (y-axis). The
1073 circles show the motif abundance and percentage H3K4me3 marked
1074 TSS's in LP up-regulated (blue) and down-regulated (red) genes (FDR <
1075 0.05; fishers two-way exact test).

1076 **Fig. 2:** *TSH β* and *EYA3* are epigenetically regulated over the season

1077 a. ChIP-seq tracks for *TSH β* gene H3K4me3 peaks across all
1078 experimental time-points. Chromosome 1 region is shown. CAGE-seq track
1079 identifying active TSS's in LP day 28 vs SP day 28. Pink represents
1080 samples in long photoperiod and marine green represents short
1081 photoperiod. Solid green boxes are canonical E-box motifs. Blue boxes are
1082 D-box motifs.

1083 b. Correlation plot for *TSH β* log2 H3k4me3 peaks from ChIP-seq versus
1084 *TSH β* log2 counts per million (CPM) from RNA-seq. Red symbols are LP
1085 sampling points, green are SP sampling points. Correlation coefficient R is
1086 shown. R=0.961, p-value=0.002. Note: SP day 28 and 84 are not included
1087 because the H3k4me3 peaks are very low.

1088 c. ChIP-seq tracks for *EYA3* gene H3K4me3 peaks. Chromosome 2 region
1089 is shown. CAGE-seq track identifying active TSS's in LP day 28 vs SP day
1090 28. Zoom in box provided to identify the downstream promoter.

1091 d. Correlation plot for *EYA3* downstream TSS log2 H3K4me3 peaks from
1092 ChIP-seq versus *EYA3* log2 counts per million (CPM) from RNA-seq. Red
1093 symbols are LP sampling points, green are SP sampling points.
1094 Correlation coefficient R is shown. R=0.778, p-value=0.02.

1095 **Fig. 3:** Identification of BMAL2 as a seasonally regulated gene

1096 a. Volcano plots showing the number of genes up (yellow) and
1097 downregulated (blue) in pairwise comparisons. The design for the
1098 comparisons is shown on the left. These plots demonstrate the
1099 consistency of the BMAL2 seasonal signal. Numbers in grey boxes are the
1100 differentially expressed genes in the pairwise comparisons
1101 (Supplementary Data 3).

1102 b. Z-score normalized log2CPM RNA-seq plots for EYA3 (blue) and
1103 BMAL2 (orange) across the whole experiment. N= 3, individual animal
1104 values are shown. Statistical significances across the season are found in
1105 Supplementary Data 3.

1106 c. Transactivation of the EYA3-downstream-TSS-luc reporter by TEF,
1107 CLOCK, BMAL1 and BMAL2. The experiment was repeated 4 times (n=4
1108 per experiment), plot displayed is a representative result. A one-way
1109 ANOVA was performed on each individual experiment using Tukey's
1110 multiple comparisons test. Different letters indicate significant differences
1111 between groups (P < 0.01). Error bars SD.

1112 d. Transactivation of the EYA3-downstream-TSS-luc reporter by TEF,
1113 CLOCK, BMAL1 and BMAL2. The lack of effect of mutating the DNA
1114 binding domain of BMAL2 is shown. The experiment was repeated 4 times
1115 (n=4 per experiment), plot displayed is a representative result. A one-way
1116 ANOVA was performed on each individual experiment using Tukey's
1117 multiple comparisons test. Different letters indicate significant differences
1118 between groups (P < 0.01). Error bars SD.

1119 e. Transactivation of the EYA3-downstream-TSS-luc reporter by TEF,
1120 CLOCK, BMAL1 and BMAL2. The effect of mutating the PAS-B domain of
1121 BMAL2 is shown. The experiment was repeated 4 times (n=4 per
1122 experiment), plot displayed is a representative result. A one-way ANOVA
1123 was performed on each individual experiment using Tukey's multiple
1124 comparisons test. Different letters indicate significant differences between
1125 groups (P < 0.01). Error bars SD.

1126 f. In situ hybridization and quantification for BMAL2 mRNA from archived
1127 material from collected every 4 hours from SP and LP. Representative
1128 images are shown (n = 4, three independent observations per animal).
1129 Error bars represent the SD. Statistical analysis by one-way ANOVA
1130 performed, different letters indicate significant differences between groups
1131 (P < 0.01).

1132 **Fig. 4:** Short photoperiods are defined by the expression of transcriptional
1133 repressors

1134 a. Experimental design: SP day 28 and LP day 28 the pars tuberalis was
1135 collected at 4 hour intervals for 24 hours. N= 3 per time-point.

1136 b. Venn diagram showing the number of diurnal genes (significantly
1137 changing throughout the day, FDR <0.05) in the PT in LP and SP
1138 (Supplementary Data 4).

1139 c. Rose plot showing the significant diurnal genes peaking at a particular
1140 phase in LP and SP. Grey bars indicate genes shared between
1141 photoperiods and yellow indicates they are unique to a photoperiod.
1142 Around the outside of the plot the durations of light and dark the animals
1143 received is plotted in grey and black respectively, the ZT times are given.

1144 d. Heatmap showing the expression profile of the genes diurnal in both SP
1145 and LP (250 genes) for each individual (n=3 per timepoint). Data are
1146 ordered by SP peak phase. Yellow is up-regulated and blue down-
1147 regulated, the data are scaled. Light dark bars are ZT times are given at
1148 the bottom of the heatmap.

1149 e. RNA-seq log2 CPM plots, n= 3, individual data shown. Grey shading
1150 indicates lights off. Statistical significances are in Supplementary Data 6.

1151 f. Transcription factor binding site analysis by peak phase in SP and LP.
1152 Grey and white shading show transition from dark and light. The arrows
1153 represent enrichment of either RORE (blue), E-boxes (pink), or D-boxes
1154 (red). The direction of arrows indicate the mean expression peak of genes

1155 containing the motif in their promoter and the length of the arrow is the -
1156 log10 p-value from a Rayleigh tests of uniformity.

1157 g. Cluster analysis of the RNA-seq data identified ZT20 SP peaking and
1158 ZT4 LP peaking gene clusters that were enriched for E-boxes. Plots shown
1159 are mean normalised log2CPM of expression profiles to visualise cluster
1160 trends. The number of genes in each cluster is indicated in the bottom left.
1161 The broken red line represents the most representative medoid gene in the
1162 cluster.

1163 **Fig. 5:** Melatonin duration defines the expression of repressor genes

1164 a. Study design. Animals were sampled at 1.5 hour intervals with either a
1165 sham implant or melatonin implant. LL= constant light.

1166 b. In situ hybridization and quantification for *CRY1* mRNA. Red bars are
1167 the value in the presence of melatonin, black bars are in constant light with
1168 a sham implant (n = 4). Representative images are shown. Statistical
1169 significances from a one-way ANOVA and are between the melatonin and
1170 sham implant at each time-point. Error bars represent the SD. P-value; * =
1171 <0.01, **=<0.001, ***=<0.0001, ****=<0.00001

1172 c. In situ hybridization and quantification for *REVERb-alpha* mRNA. Red
1173 bars are the value in the presence of melatonin, black bars are in constant
1174 light with a sham implant (n = 4). Representative images are shown.
1175 Statistical analysis by one-way ANOVA performed, different letters indicate
1176 significant differences between groups (P < 0.01). Error bars represent the
1177 SD.

1178 d. As in c for *CHRONO* mRNA.

1179 e. As in c for *DEC1* mRNA.

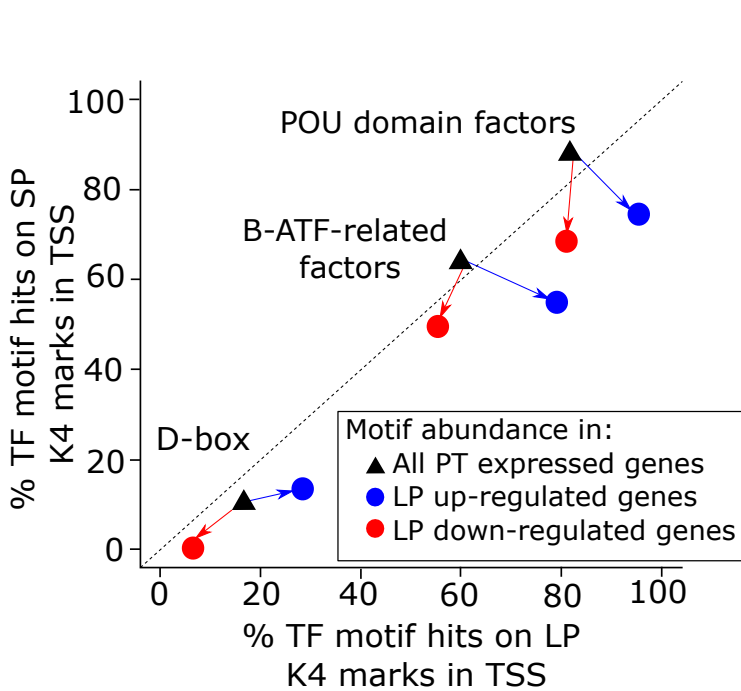
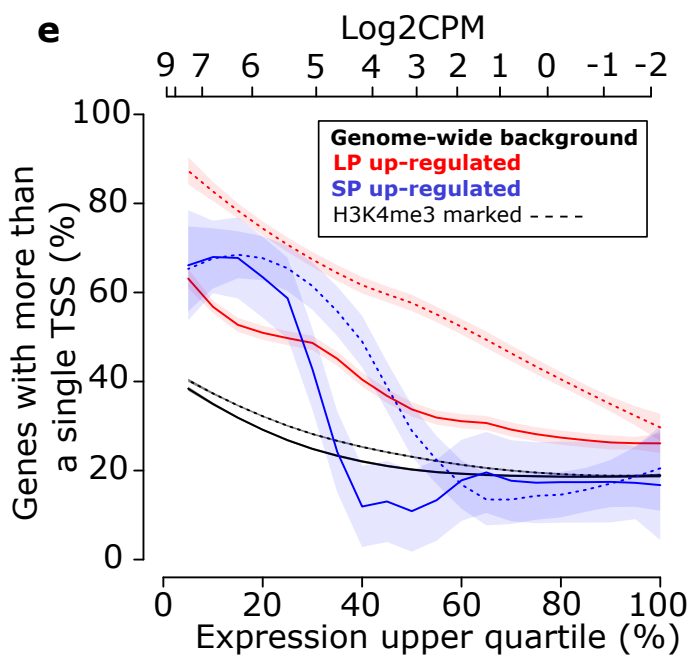
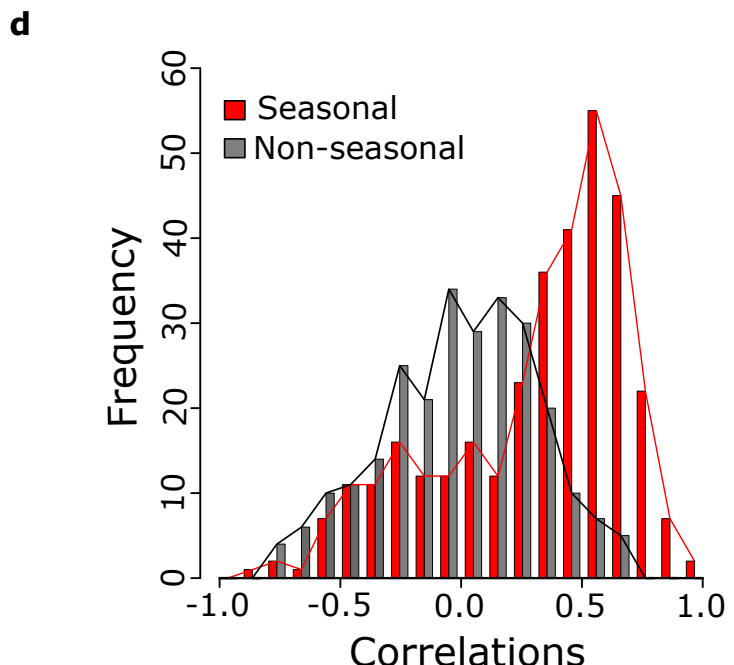
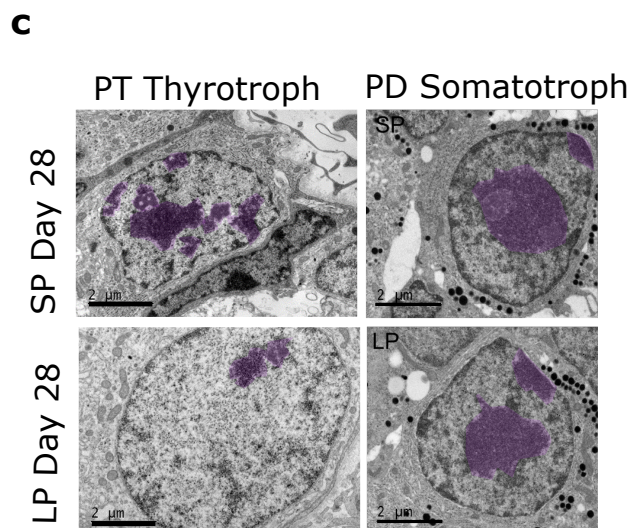
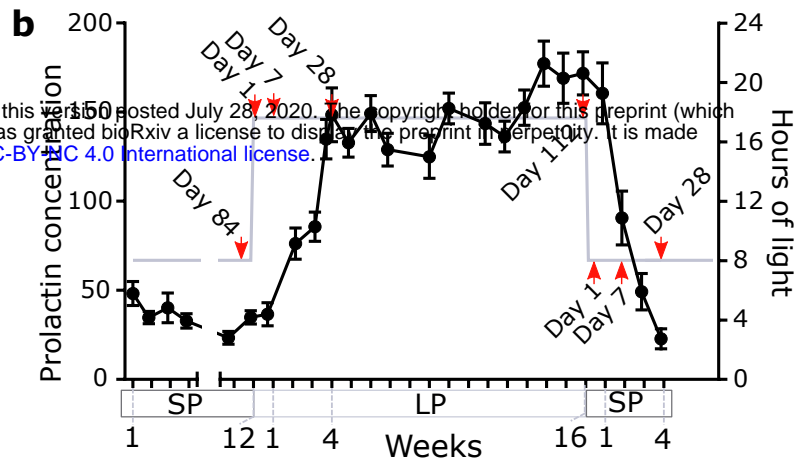
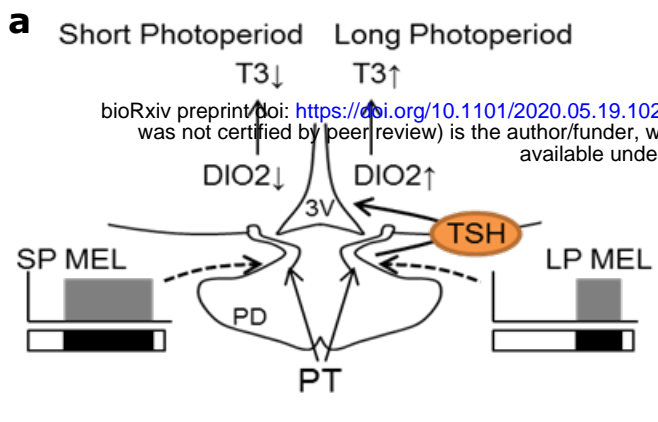
1180 f. In situ hybridization and quantification for *DEC1* mRNA from archived
1181 material from collected every 4 hours from SP and LP (n = 4).
1182 Representative images are shown. Error bars represent the SD. Statistical
1183 analysis by one-way ANOVA performed, different letters indicate
1184 significant differences between groups (P < 0.01).

1185 g. Double immunohistochemistry for DEC1 (red), aGSU (green) and dapi
1186 nuclear stain (blue). White arrow heads indicate FS cells. Scale bar 20um.

1187 h. Transactivation of the EYA3-downstream-TSS-luc reporter by TEF,
1188 CLOCK, BMAL1 and BMAL2 is repressed by DEC1. The experiment was
1189 repeated 4 times (n=4 per experiment), plot displayed is a representative
1190 result. A one-way ANOVA was performed on each individual experiment
1191 using Tukey's multiple comparisons test. Different letters indicate
1192 significant differences between groups ($P < 0.01$). Error bars SD.

1193 **Fig. 6:** Mammalian photoperiodism model: coincidence timing and epigenetic
1194 regulation

1195 The photoperiod sculpts the duration of the melatonin signal, long duration on
1196 short photoperiods (SP, winter) and short duration on long photoperiods (LP,
1197 summer). In the pars tuberalis approximately 12 hours after the onset of
1198 darkness there is a photosensitive phase. When this phase coincides with
1199 light BMAL2 is expressed. When this phase is coincident with darkness DEC1
1200 is expressed. This forms a photoperiodic flip-flop switch between two stable
1201 states. The role of BMAL2, CLOCK and BMAL1 is to co-activate EYA3 and
1202 subsequently seasonal physiological changes. DEC1 suppresses the E-box
1203 based activation of EYA3. Also occurring in the dark phase of SP a number of
1204 repressors are expressed which target appear to target LP induced genes
1205 potentially inhibiting the expression of summer physiology. Aside from this
1206 acute photoperiodic flip-flop switch there is a progressive photoperiod
1207 dependent epigenetic regulation over a number of weeks augmenting the
1208 coincidence based timer drive on summer physiology.



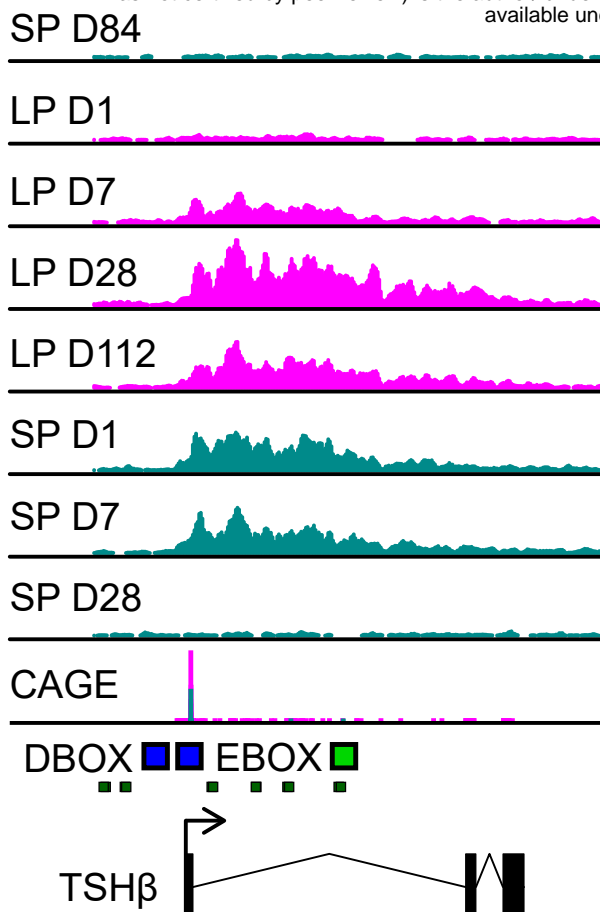
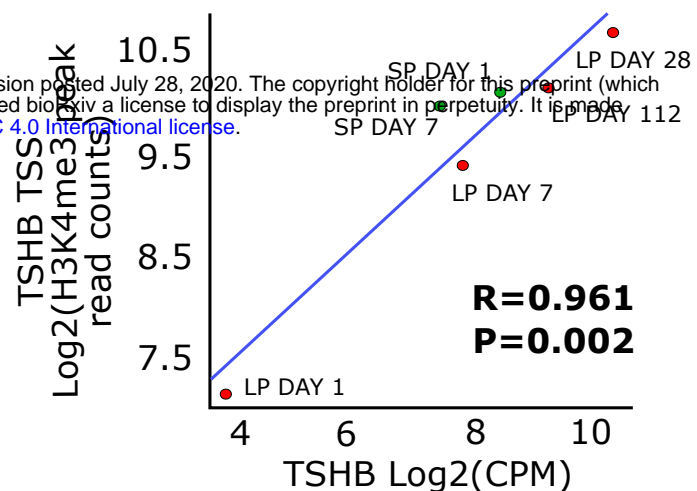
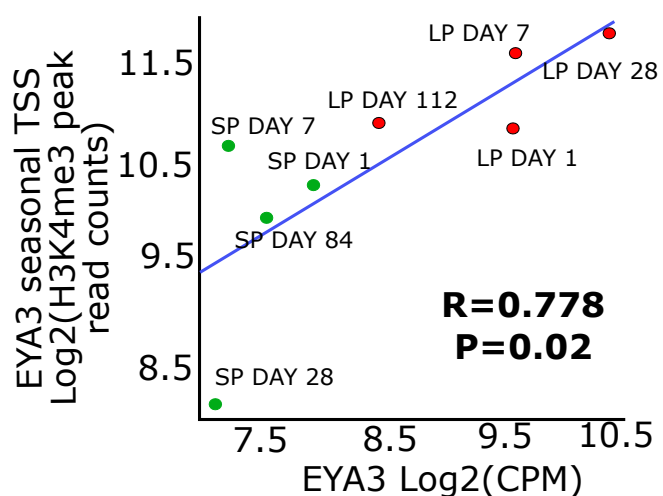
aTSH β H3K4me3

97228

97232

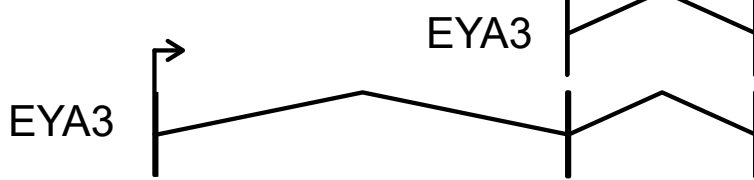
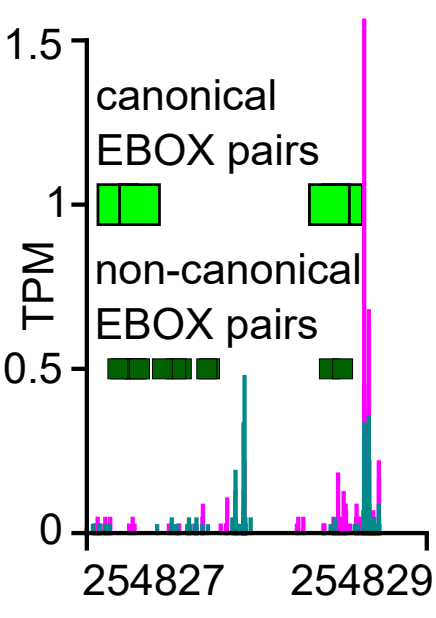
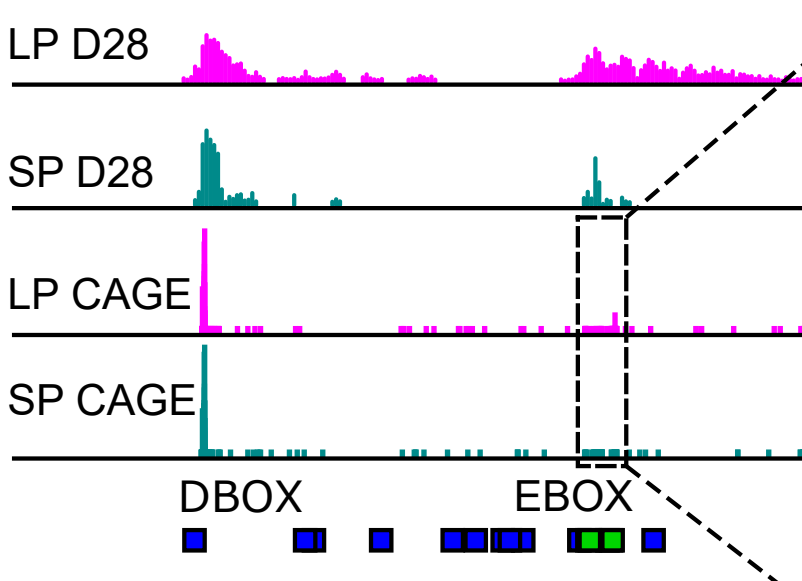
97236

bioRxiv preprint doi: <https://doi.org/10.1101/2020.05.19.202194>; this version posted July 28, 2020. The copyright holder for this preprint (which was not certified by peer review) is the author/funder, who has granted bioRxiv a license to display the preprint in perpetuity. It is made available under aCC-BY-NC 4.0 International license.

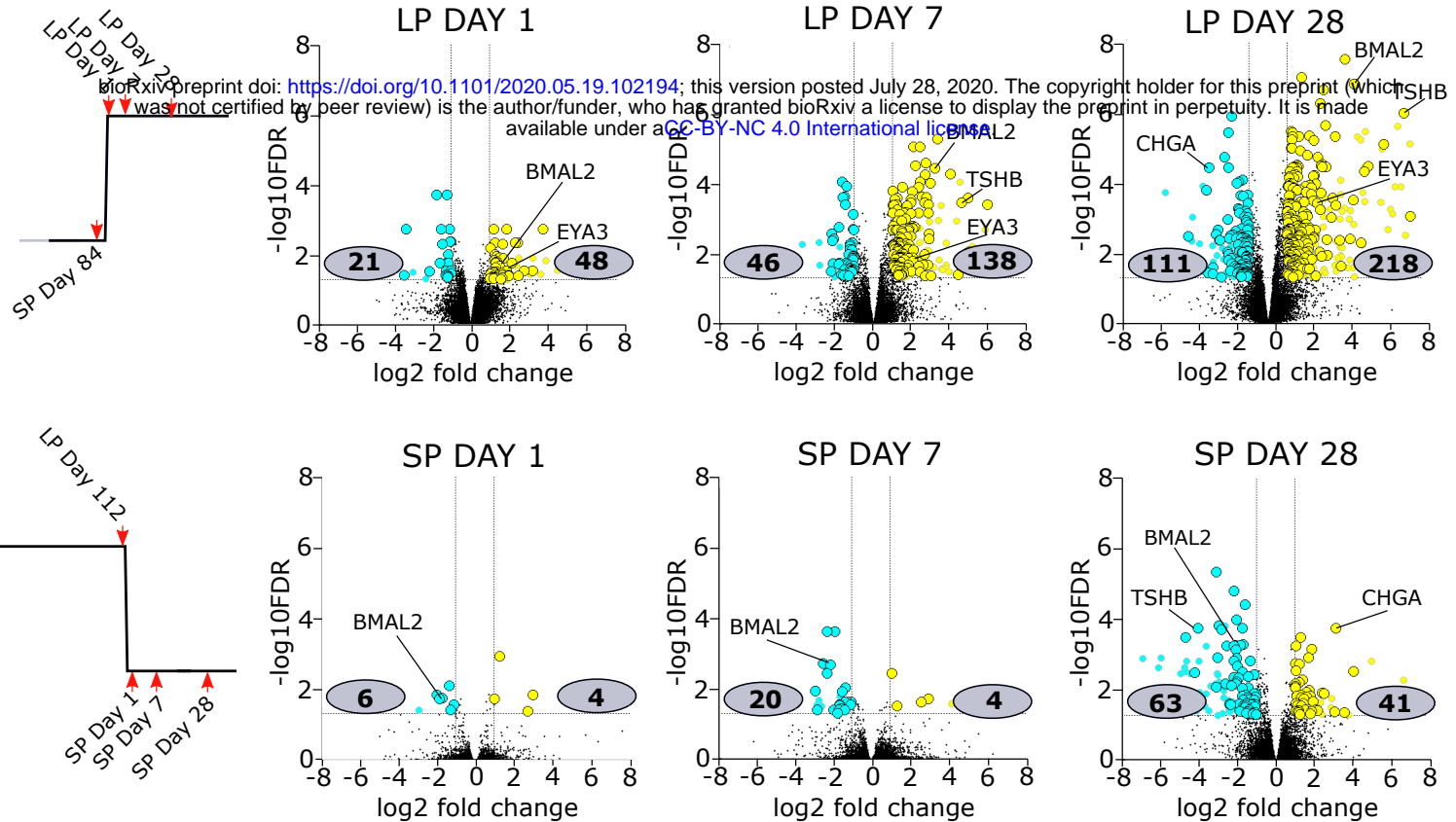
**b****d****c**

EYA3 H3K4me3

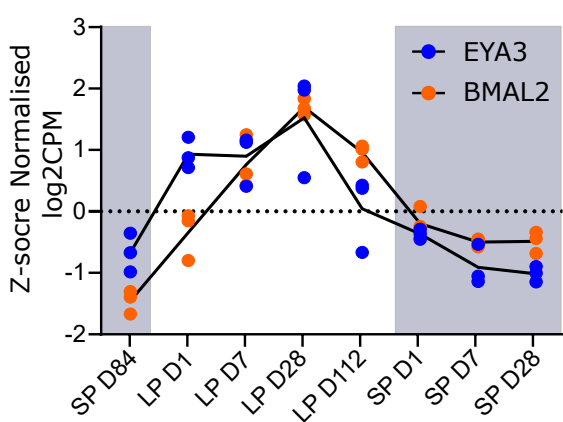
254800 254820 254840



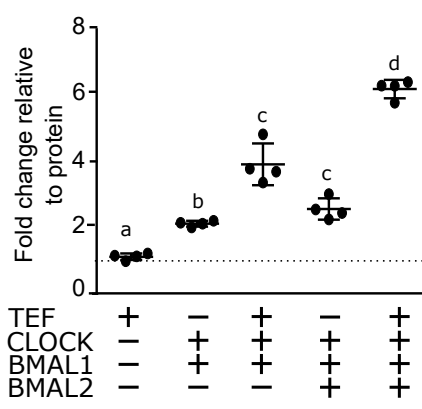
a



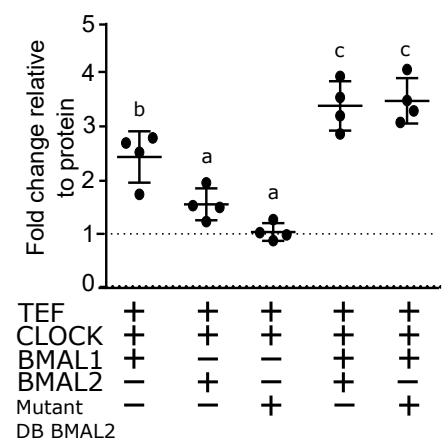
b



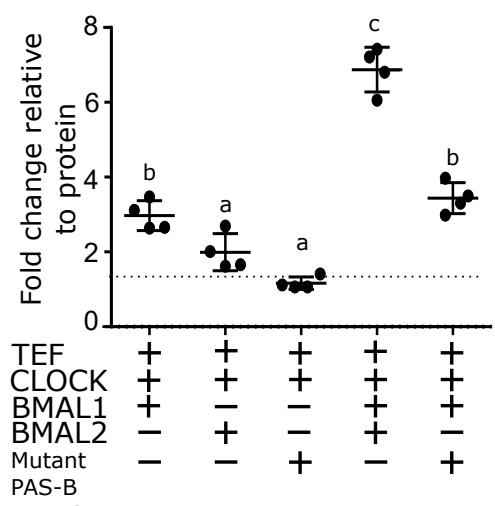
C



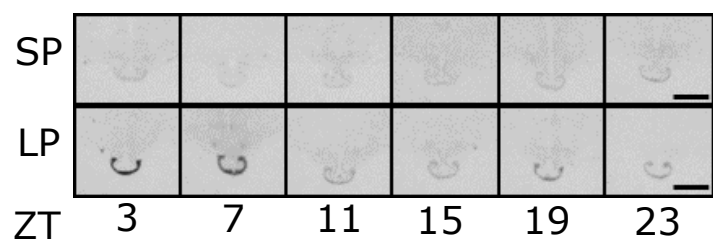
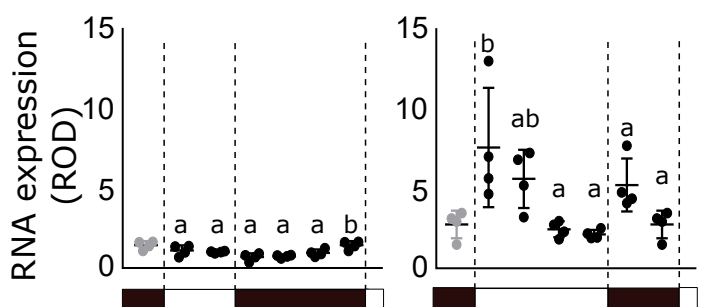
d



e

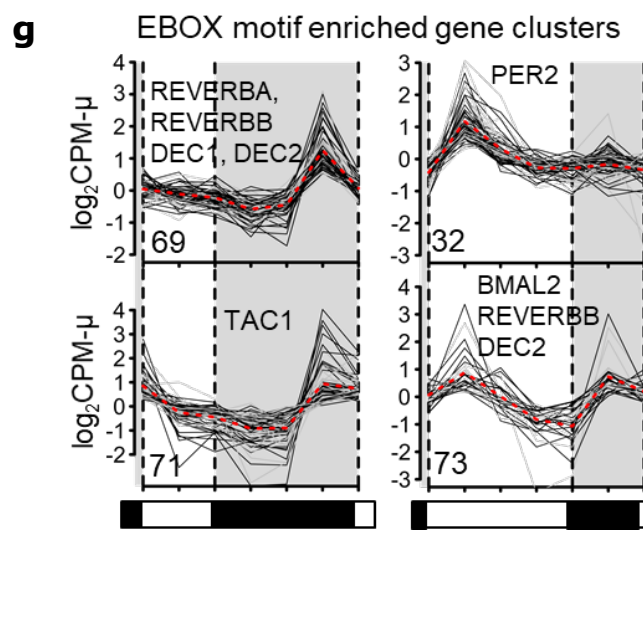
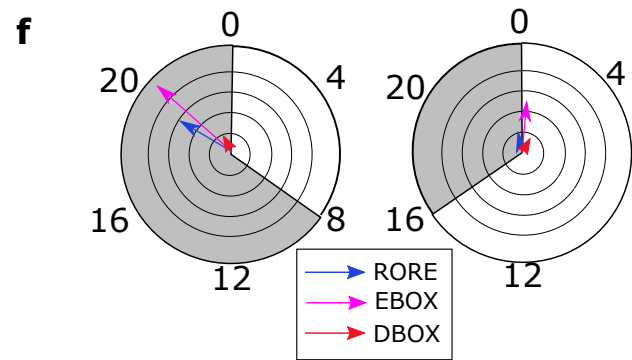
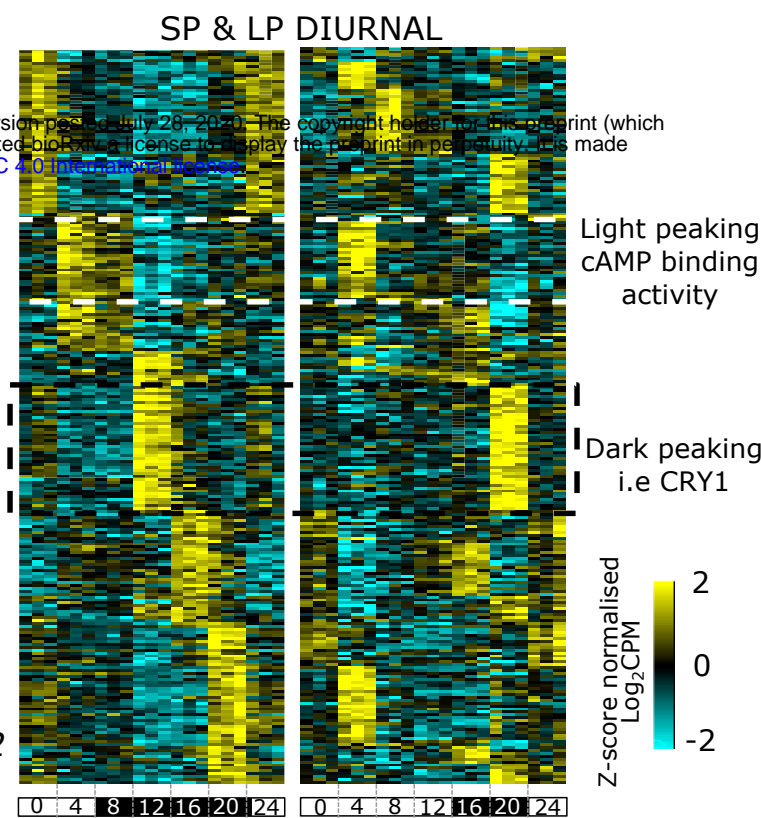
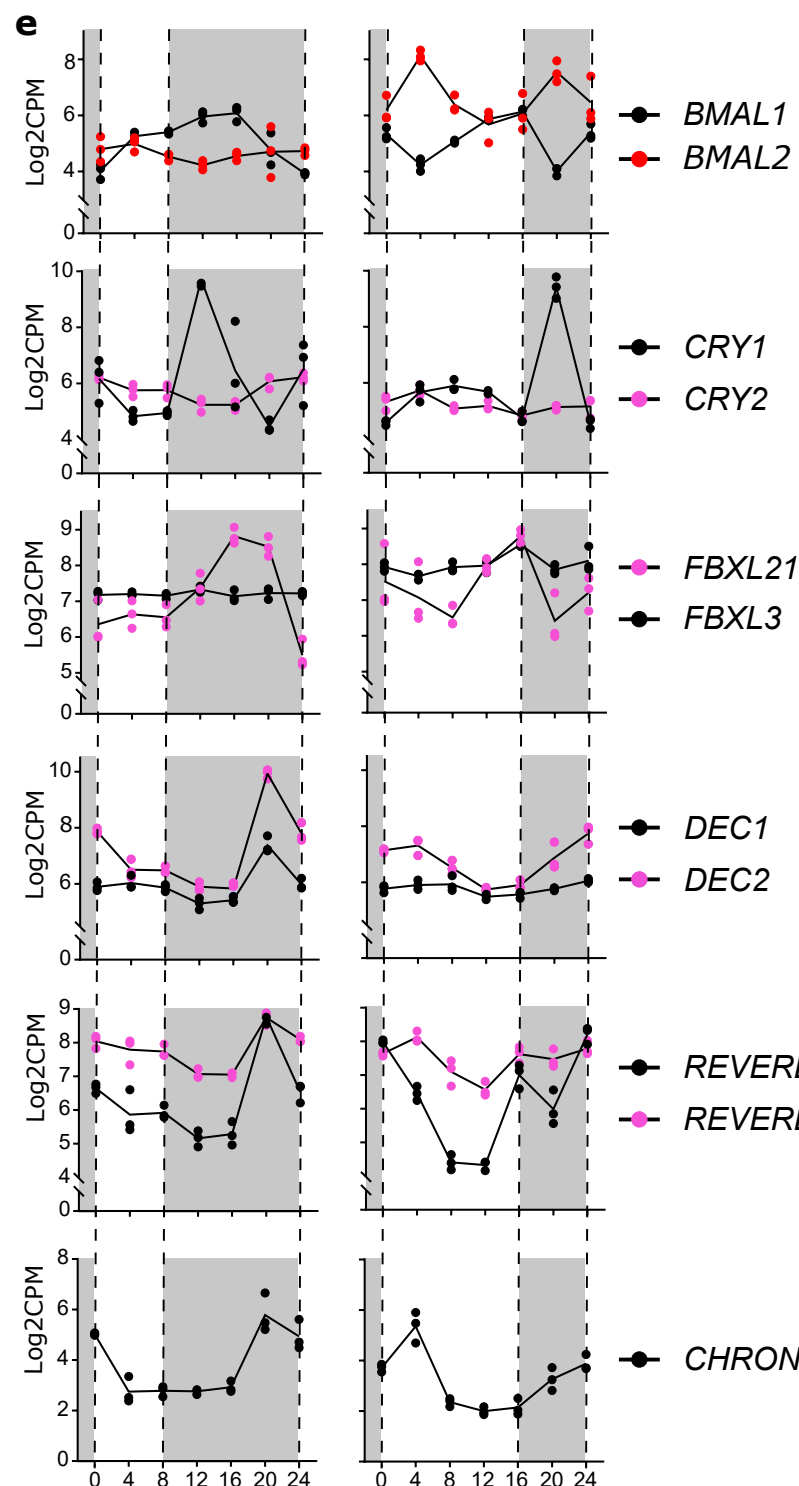
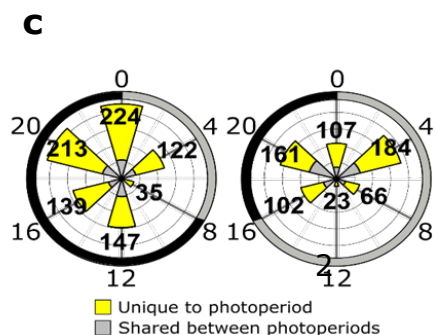


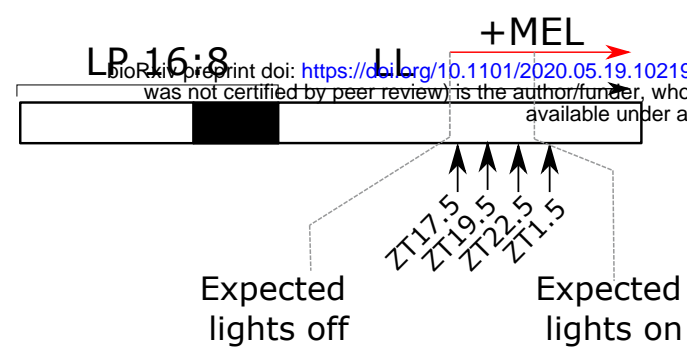
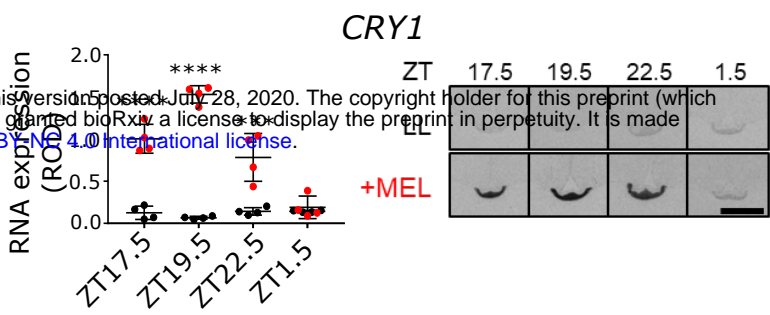
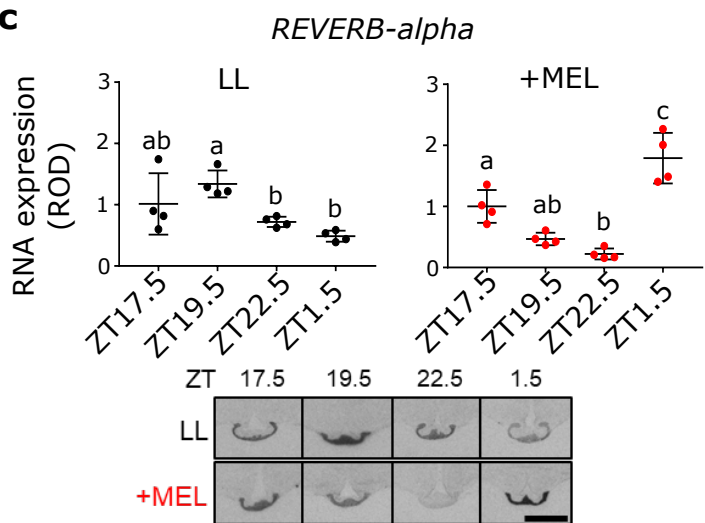
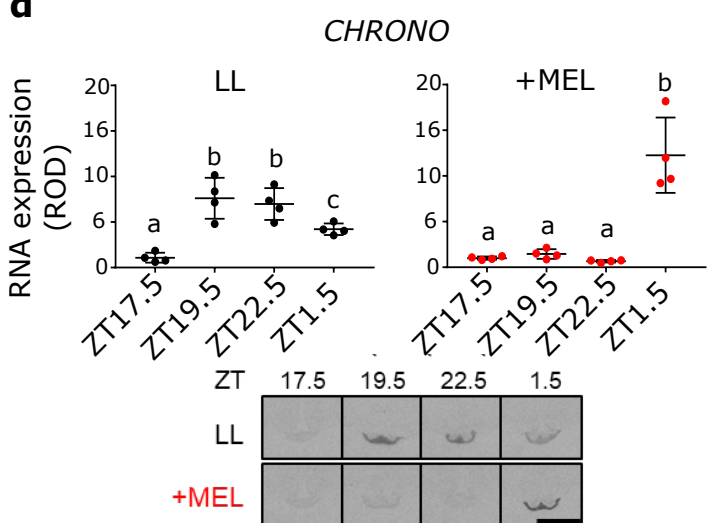
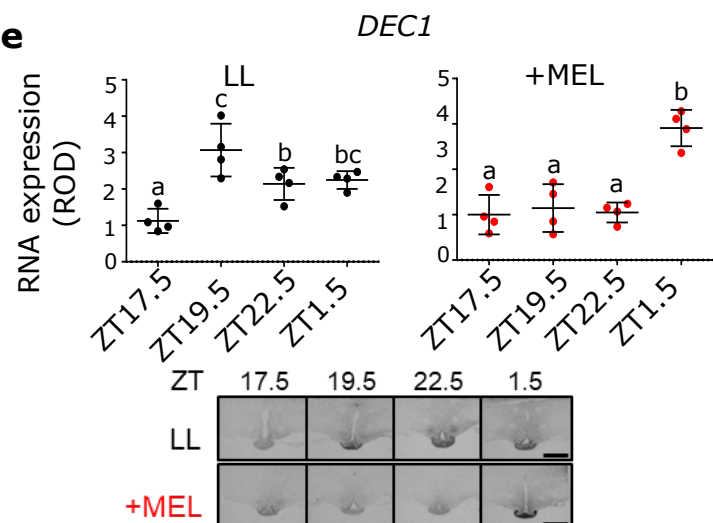
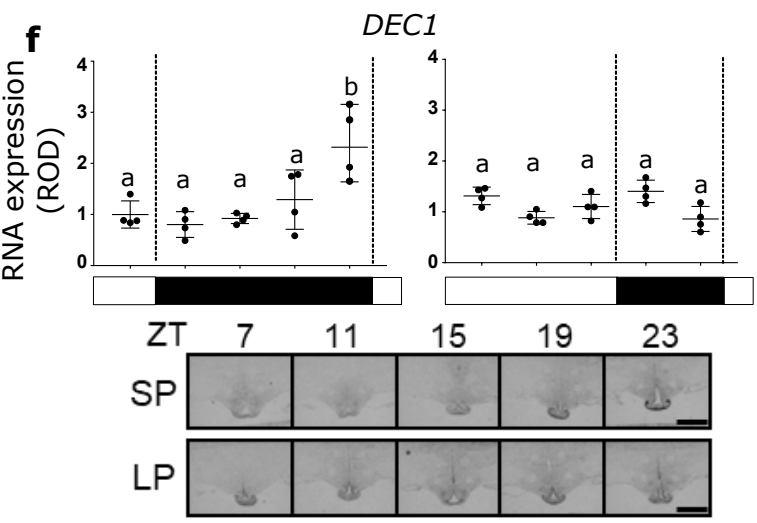
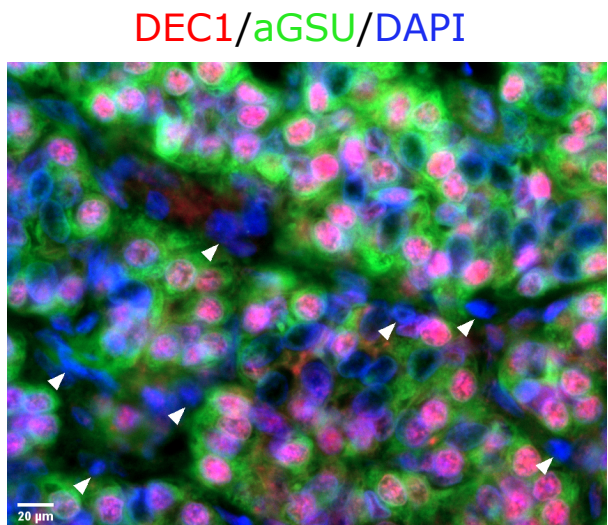
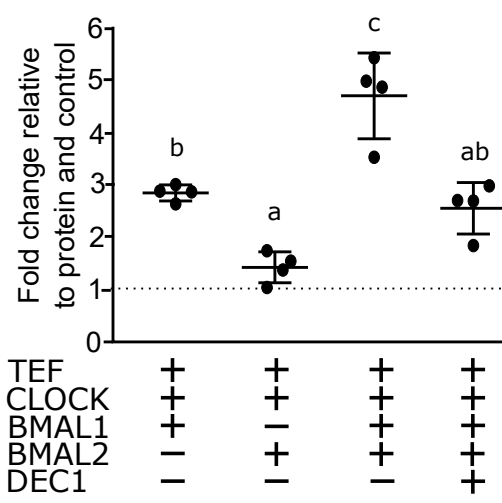
f





bioRxiv preprint doi: <https://doi.org/10.1101/2020.05.19.102194>; this version posted July 28, 2020. The copyright holder for this preprint (which was not certified by peer review) is the author/funder, who has granted bioRxiv a license to display the preprint in perpetuity. It is made available under aCC-BY-NC 4.0 International license.

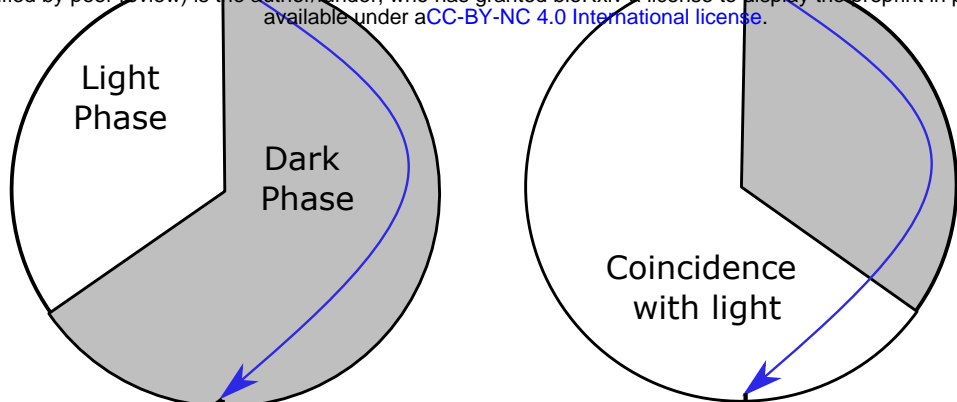


a**b****c****d****e****f****g****h**

Winter

Summer

bioRxiv preprint doi: <https://doi.org/10.1101/2020.05.19.102194>; this version posted July 28, 2020. The copyright holder for this preprint (which was not certified by peer review) is the author/funder, who has granted bioRxiv a license to display the preprint in perpetuity. It is made available under aCC-BY-NC 4.0 International license.



Coincidence timing

- Photoperiod
- Summer gene promoter accessibility
- Summer gene expression

Summer physiology

Photoperiod dependent epigenetic regulation

